Report No. TATRC-TRON-02
Project Title: Telesurgical Robotic Operative Network (TRON)
Project ID: XV5-3B_19_0002

Final Report – Telesurgical Robotic Operative Network (TRON)

Prepared By:
Ethan Quist, Jaeyeon Lee, Nathan Fisher

Telemedicine and Advanced Technology Research Center

Medical Robotics and Autonomous Systems Division

August 2023

Table of Contents

Contents

Telesurgical Robotic Operative Network

Executive Summary

The Telemedicine and Advanced Technology Research Center is charged with the mission to fuse data, humans, and machines into trustworthy solutions that optimize medical performance and casualty outcomes. The Medical Robotics and Autonomous Systems (MedRAS) division within TATRC strives to accomplish this through the development and advancement of robotic systems and applying them to casualty care. With timely surgical intervention being one of the most important indicators for casualty survival and future operating conditions leading to a wider dispersion forward deployed surgical expertise there arose a need for novel surgical paradigms for future battles. The TATRC MedRAS team strove to investigate and develop a novel surgical assistive robotic platform by leveraging advancements in robotic control, network engineering, and computer vision while partnering with the leading industry and academic experts in surgical robotics. This report details the entirety of the Telesurgical Robotic Operative Network (TRON) project, highlighting major accomplishments from the main aims and objectives. Research contributions from TATRC, SRI International, and our university partners the University of California San Diego (UCSD), the University of California Berkeley (UCB), and the University of Chicago (UC) are all documented throughout this report. A proof-of-concept live animal study where the developed robotic platform assisted in a temporary vascular shunt placement procedure concluded the TRON project. This report includes details of the animal study as well as discussion of the results and key takeaways.

Section 1.1: Project Background

The goals of the Telesurgical Robotic Operative Network (TRON) project are to identify and characterize the problems caused by signal latency in telesurgical robotics, and to investigate methods that effectively mitigate these problems to provide safe and effective robotic telesurgery. Our approach focuses on the design of semi-autonomous robotic surgery protocols and application of machine learning to improve the performance and safety of complex robotic surgical tasks in the setting of time delay and signal disruption. Our hypothesis is that semi-autonomous protocols and applied machine learning are effective countermeasures to improve the safety profile and efficacy of robotic telesurgery against excessive signal latency and signal disruptions.

Summary of Research Objectives:

1) Investigate the deleterious effects of signal latency on standardized and validated robotic surgical tasks in virtual simulation and real-time using a robotic tele-surgical platform

2) Research and design optimal machine learning strategies and algorithms (supervised learning vs unsupervised learning vs reinforcement learning) for application to robotic surgical tasks and procedures.

3) Research and design semi-autonomous robotic assistance protocols that can increase the efficiency, precision, and safety while maximizing surgeon-control under extensive signal latency and signal disruption.

The development and implementation of telerobotic surgical capabilities to support prolonged field care under the Army's future Multi-Domain Operations (MDO) concept is hindered by time-delays incurred by satellite networks and complex signal transmission across long geographic distances [1]. Latency is an especially unique challenge with teleoperated surgical systems because of the bi-directional nature of communications, the need for real-time communication of commands and immediate feedback. A baseline level of signal latency is inherent with telerobotic surgery; however, latency increases of even tens of milliseconds can cause surgeon-control to deteriorate to an unsafe level.

Two research strategies for addressing the communications latency problem in telerobotic surgery are 1) address signal transmission performance (latency, jitter, and bandwidth) caused by data compression and satellite delays directly, OR 2) compensate for expected network latency and bandwidth limitations by augmenting teleoperated control with local perception and tactical feedback analysis at the remote patient location with immediate autonomous robotic response. The research conducted for this project focused mainly on the second approach, e.g., applying autonomy to the telesurgical robotic system as a countermeasure to network latency and bandwidth limitations. The first approach of addressing network performance issues directly is not the focus of this research because this is not an issue that is specific to medical applications and is actively being addressed by the signal community.

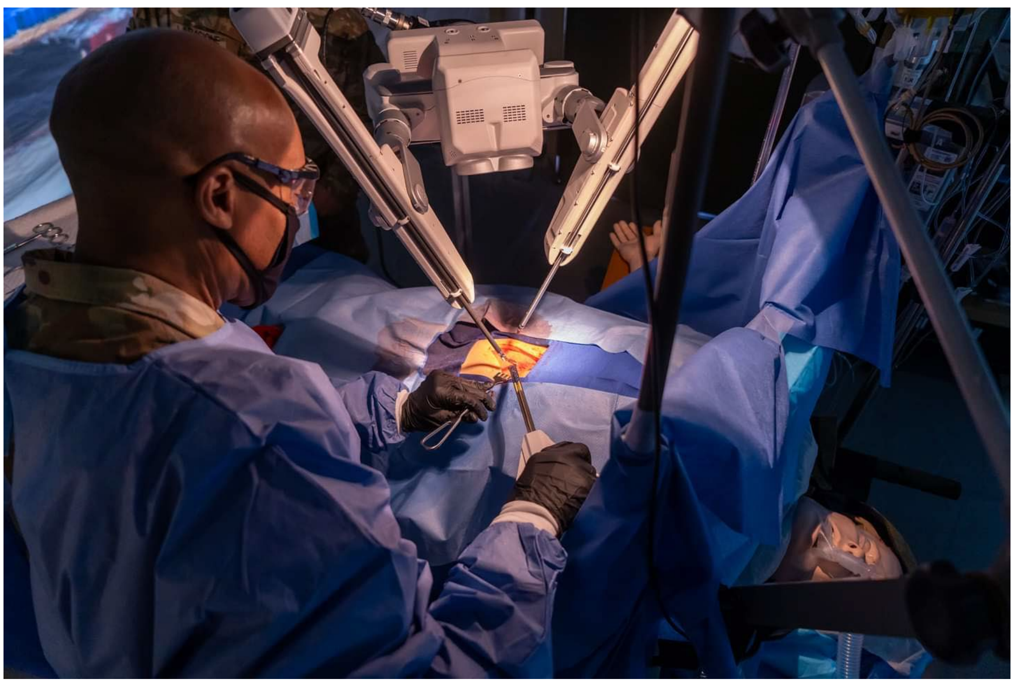

Figure 1. Taurus-M surgical assist robot in a simulated procedure.

In this project we successfully prototyped and demonstrated semi-autonomous protocols, designed using machine learning and computer vision, to robotic surgical tasks at the remote location to minimize the effects of signal latency and thereby improve the safety profile and efficacy of robotic telesurgery. The purpose of this project was to identify and evaluate the problems caused by signal latency in telesurgical robotics, and to develop solutions that effectively mitigate these problems to provide safe and effective robotic telesurgery. Our research accomplished establishing a semi-autonomous robotic framework that enables safe and effective telesurgery by accommodating for the deleterious effects of signal latency and providing autonomous actions in response to signal disruptions. Countermeasures to signal latency and signal disruption were investigated and a proof-of-concept solution to mitigate these effects was developed through the application of autonomous behaviors to the robotic system at the remote patient location. Our end objective was a prototype capability that enables the conduct of various surgical tasks and procedures through supervised autonomy (semi-autonomy) and application of machine learned protocols that allow for dynamic improvements and refinement of techniques. The goal was to minimize the complexity and bandwidth required to perform surgical procedures such that the performance and safety of complex robotic surgical tasks can continue to be performed in remote field settings where signal latency and disruption would otherwise preclude telerobotic surgery.

To demonstrate our success, we concluded this project with a live animal study where our developed telerobotic surgical prototype assisted in a temporary vascular shunt placement procedure. This procedure was targeted because it represented a battlefield relevant intervention that requires more than one surgeon, and the expertise of a vascular surgeon to complete. The goal of this project was to demonstrate that surgical expertise can be projected forward to the point of need and successfully assist a surgical team despite the deleterious effects of signal latency encountered with the geographic distance between robot and remote expert surgeon. We achieved these aims by demonstrating our semi-autonomous surgical robotic framework in successfully assisting in a vascular shunt placement procedure while under the effects of high signal latency.

Figure 2. The Taurus-M surgical assist robot.

Section 2.1: Preliminary Latency Study

Investigating Effects of Signal Latency on Surgery

In the first year of the project the Co-PI from Walter Reed National Medical Center, MAJ Steve Hong, conducted and published a research study into the deleterious effects of signal latency on standardized and validated robotic surgical tasks in virtual simulation and real-time using a robotic telesurgical platform [2]. Using the Da Vinci Research Kit (dVRK) at the University of California San Diego (UCSD), Dr. Hong, and partner clinician Dr. Ryan Orosco performed multiple Fundamentals of Laparoscopic Surgery (FLS) standardized tasks at varying levels of inserted latency and documented their findings. One aspect of their study was investigating the impact motion scaling had on improving task time and error rates. They found that performance declined with increasing time delay. Statistically significant increases in task time and numbers of errors were seen at 500ms and 750ms delay. In their study they found total errors were positively correlated with task time on linear regression. Under 750ms of delay, negative instrument motion scaling improved error ratios. They concluded that above 750ms of delay it was unsafe to directly teleoperate a robotic system to lead a surgical intervention, however there are promising methods of mitigating the deleterious effects of latency such as motion scaling and other Machine Learning adaptations to surgical robotic control.

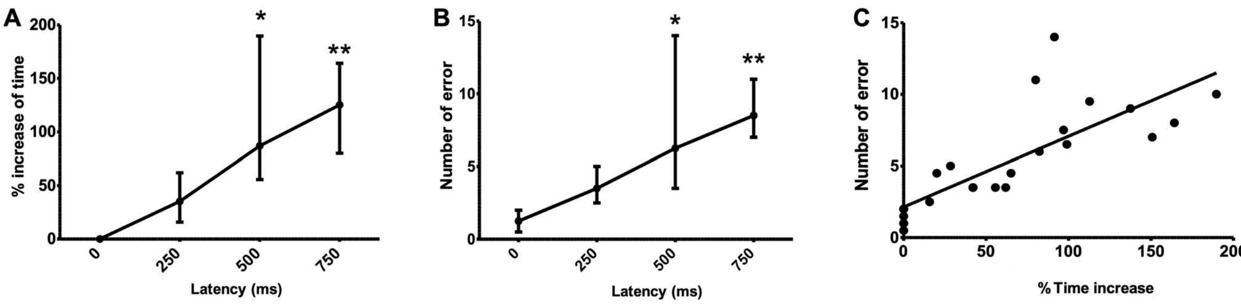

Figure 3. Results from Dr. Hong & Dr. Orosco's study into latency's effect on errors and completion time of teleoperated surgical robotic tasks.

Section 2.2: Hardware Design

Taurus-M

In December of 2020, SRI International delivered to TATRC the Taurus-M surgical robot platform that would be used for the rest of the TRON project. The original Taurus robot was developed by SRI for a project funded by the Department of Homeland Security to safely diffuse explosive ordnance from a safe distance. SRI designed a small form factor teleoperated robot with a high level of dexterity in the arms and wrists to accomplish complex grasping and maneuvers at the robot's grippers. A remote operator controls the robot through a Virtual Reality (VR) headset, within a virtual digital control room called the Operator Control Unit (OCU). In this design, the VR's hand controllers directly map to robot arm and wrist movements. The Taurus's design was ideal to be adapted for telerobotic surgery. SRI redesigned the arms of the Taurus robot to equip the Da Vinci Xi line of state-of-the-art surgical robotic tools. The robot arms function as tool adapters, allowing for surgical tools to be hot swapped in and out during operation. This allows for the entire range of the Da Vinci catalog to be used with the Taurus robot, turning it into a surgical Swiss Army Knife. The Taurus-M (medical), as it is now called, weights under 20 lbs., has a small footprint of 2ft x 2ft, and runs off simple 120V wall power. The robot's low SWAP-C design is uniquely fit for forward rapid deployment as it is portable, easy to set up and tear down, and draws a relatively low amount of power. Starting in 2021, the team at TATRC was able to utilize the Taurus-M robot for the remaining in-lab preliminary studies leading up to the animal study at the end of the project in March 2023.

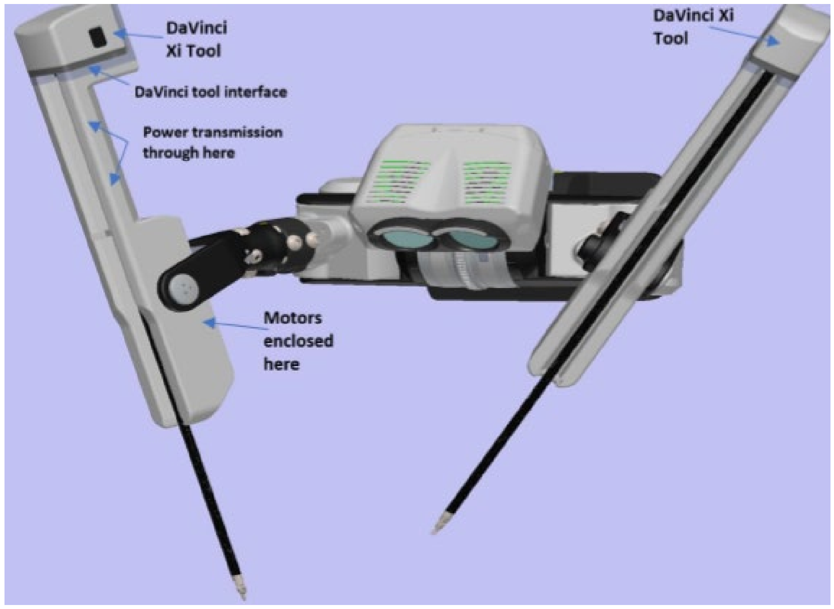

Figure 4. System design of the Taurus-M surgical assist robot.

Section 2.3: Remote Operation

System Design

Different from complex operating room surgical robotics that require multiple modules, intricate wiring, and professional setup, the Taurus-M is a single robotic platform with a small footprint. This makes it particularly appropriate for mobile surgical facilities that may lack the infrastructure necessary for commercial surgical robot systems. Additionally, it facilitates telepresence surgery, enabling field surgeons to establish remote connections and receive expert assistance or specialized care. This becomes especially crucial in mass casualty situations where immediate access to specialized surgeons may be limited. By remotely connecting to the Taurus-M stationed at a forward medical facility, field surgeons can receive remote guidance and support from off-site specialists. This connectivity ensures that critical expertise is accessible even when the specialist cannot be physically present. The Taurus-M's telepresence capabilities enhance the capabilities of field surgeons and improve patient outcomes, particularly in challenging circumstances.

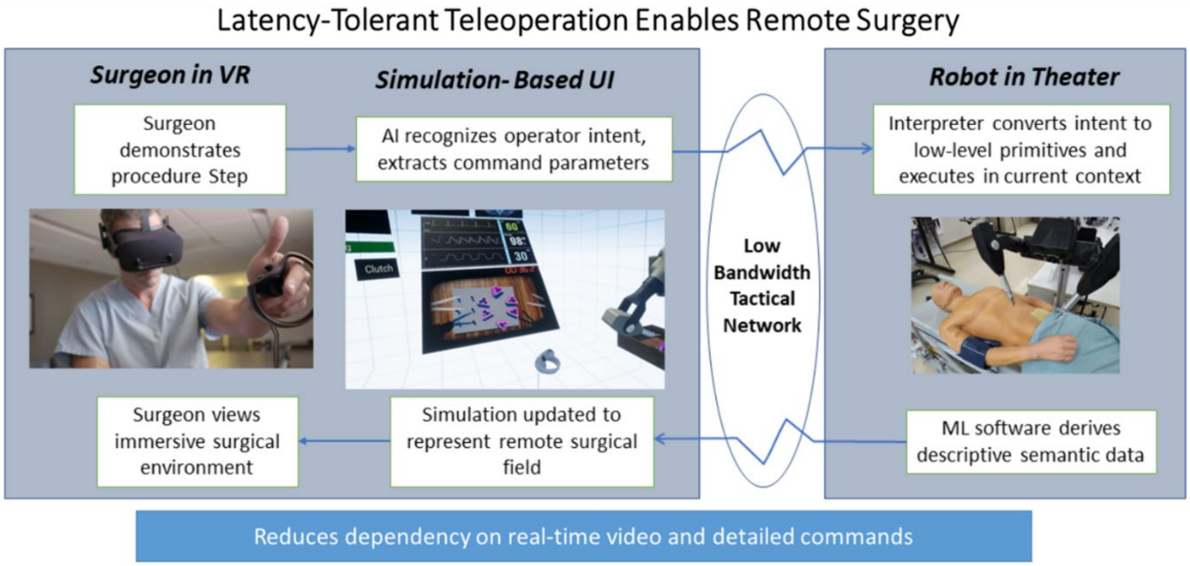

Figure 5. System description of the Taurus-M surgical platform. The remote surgeon operates inside a Virtual Reality based digital environment while teleoperating the surgical robot from afar.

Cross-Country Control Testing

In October of 2021 the teams at TATRC and SRI began work on attempting to demonstrate the ability to remote control the robot from another installation. Quick success was achieved at controlling the simulation software in a distributed control framework from SRI, in Palo Alto CA, to UCSD, in San Diego CA. Researchers in San Diego were able to conduct a FLS peg board procedure wearing the Virtual Reality headset, while the software was hosted in Palo Alto CA. A repeated exercise was attempted from Fort Detrick, Maryland, to the same simulation software hosted at Palo Alto, CA. Significant barriers were encountered regarding government firewalls preventing the access to SRI's simulation environment. Once the firewall barriers were overcome, the researchers at TATRC were able to successfully control the simulation software in CA from the VR headset in MD. The control however was significantly hindered by the 3,000 miles of geographical distance and encountered latency and packet loss. The insights into this exercise informed SRI the need to reinforce their robot control framework to be more robust to packet lost and packets arriving out of order.

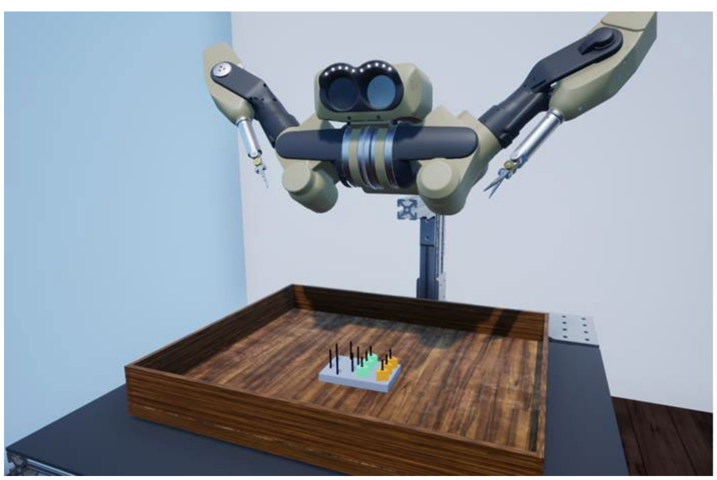

Figure 6. The Taurus robot in a digital simulation environment of the FLS peg board task.

Section 2.4: Robotic Framework

System Architecture

Throughout the period of performance SRI and the university research partners were hard at work updating and adapting the robotic framework of the Taurus-M robot to be a capable telesurgical robotic platform. A system architecture was defined in the Summer of 2019 where the robot would operate in a distributed control scheme, with local robot control running on a computer stationed with the robot, and operator commands are interpreted from the Virtual Reality (VR) Operator Control Unit (OCU) stationed with the remote surgeon. Figure 7 illustrates the system architecture of the Taurus-M. Control is divided between the operator side and the robot side with compute capability at both sites and the ability for communication in-between even in low-performance networks. At the Operator Side visualization of the surgical side is received from the Robot-Side world simulator using developed perception technologies. Semantic model changes are also received to update the simulated surgical site based on computations made on the Robot Side. The surgeon at the Operator Side uses the VR hand controllers to make operator intent commands of surgical action and the system sends them to the Robot Side. At the Robot Side, the control system receives the operator intent commands and translates them into motor control commands to drive the robot. The robot state messages are send back from the robot's motors to the robot controller, which then drives the semantic model changes back to the Operator Side visualization of the surgical site. This framework has been proven to work with the robot operating in pure simulation for training, in direct teleoperation mode, and also in the developed semi-autonomous control framework.

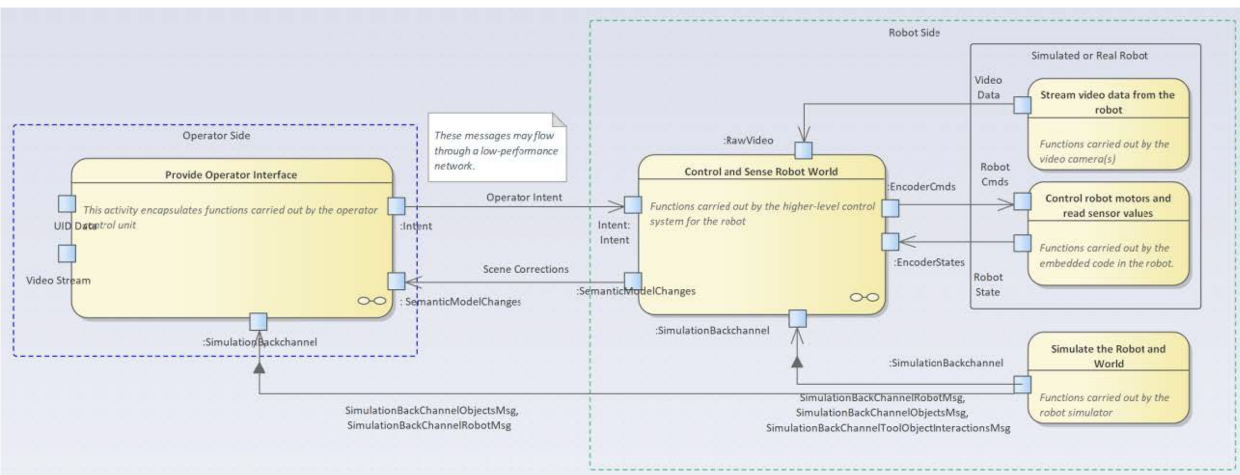

By September of 2020 the software architecture was implemented in the Taurus-M robot at TATRC allowing the research team to test the robot's capabilities in the TATRC lab on Fundamentals of Laparoscopic Surgery (FLS) standardized tasks and simulated tissue. Later in the project timeline, the software was homogenized to the universally used Robot Operating System (ROS) architecture to allow the platform to be a more attractive research platform for future opportunities and partners. Adapting to ROS also allowed for a smoother distributed control scheme between multiple computer stations and even reduced inherent latency in the system. Additional small upgrades were continuously added to the VR OCU, such as upgrading the Unreal Engine (UE) backbone of virtual reality environment to version 4.21. SRI finished their software architecture in the last year of the project by investigating migration to OpenXR with the goal of supporting hardware other than Meta Oculus products. Alternative products such as HP Reverb G2 and Samsung VR have been considered.

Figure 7. (left) the remote surgeon operating through the Oculus Rift S Virtual Reality headset and (right) the Operator Control Unit digital display within the VR headset that provides stereoscopic view from the robot and situational awareness on the robot's pose, vitals from the patient, and even a possible bird's eye view of the operating room.

Section 2.5: Surgical Perception

Surgical Anatomy and Object Detection

The main focuses for the university partners at University of California San Diego (UCSD), University of California Berkeley (UCB), and University of Chicago (UC), were to develop surgical perception tools to enable Artificial Intelligence (A.I.) and surgical autonomy in the robotic framework. UC throughout the project focused on developing perception technologies to identify and segment anatomy in the surgical scene. UC started by identifying and segmenting the pegs and triangles of the FLS peg transfer task.

To perform accurate object detection and segmentation UC needed to accomplish three main steps: color and texture masking, contour detection, and polygonal orientation detection. UC was able to successfully fine tune a computer vision color and texture masking algorithm that was accurate up to minor pixel-level errors. By dividing the image into different object classes and defining specific color and texture ranges for those object classes they were able to, with high accuracy, segment the FLS colored triangles from the FLS pegs and the background. This method translated to identifying vessels in a surgical scene but required much finer tuning of the color and texture ranges for anatomy object classes. Contour Detection first utilized an unsupervised learning Machine Learning module to cluster pixels together into a desired number of "course objects". Then a contour detection algorithm refines the objects into a finer-grained pixel boundary. Lastly UC's Polygonal Orientation Detection algorithm uses computational geometry algorithms to fit polygonal splines to the contours based on a shape prior for each of the objects. This detects vertices and principal axes which provide vital 3-D orientation information to build semi-autonomous grasping motions.

After successfully segmenting all the relevant objects for the FLS peg transfer task, they adapted their perception software for the temporary vascular shunt procedure. The new tissue segmentation software was successfully able to identify vessels in the scene and segment the vessel edges. Identifying the edges of the vessel opening was important for a vascular shunt placement procedure because the robot needs to identify correct grasping locations along the vessel edge to conduct the procedure. UC's code could identify in 3-D space two ideal locations for the robot to grasp on the vessel edge.

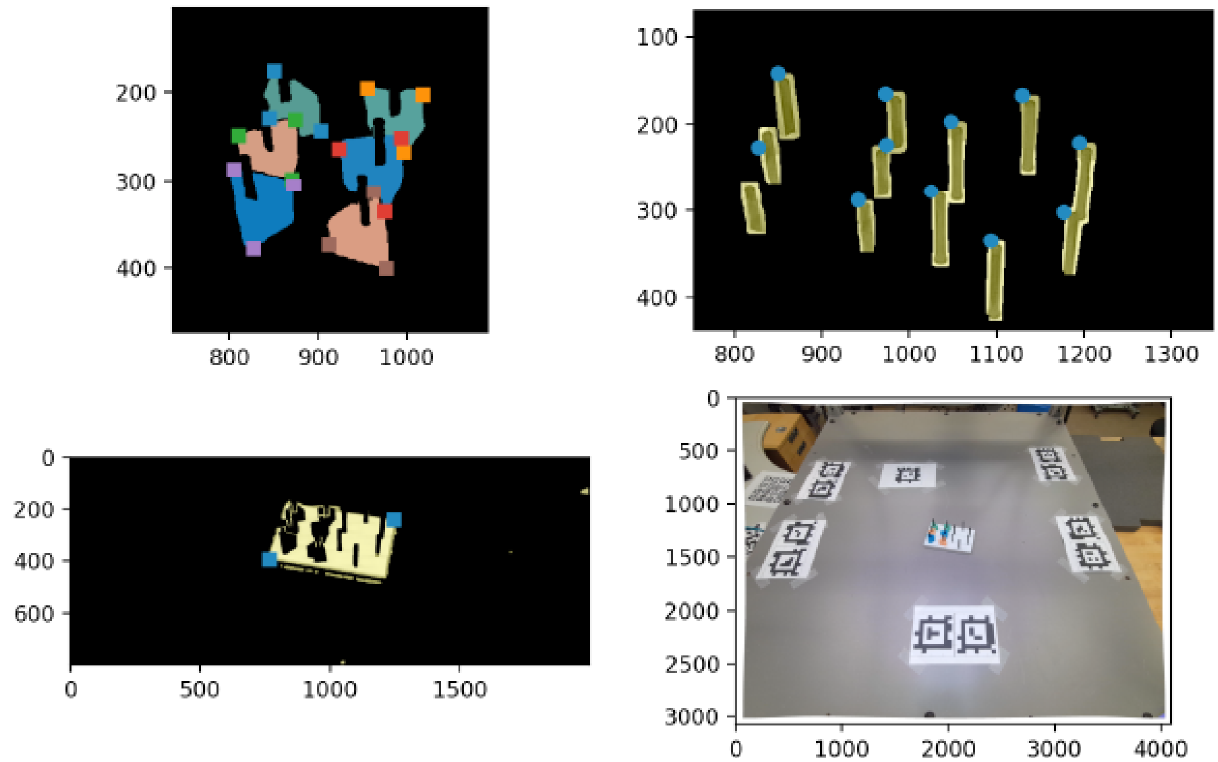

Figure 8. University of Chicago's segmentation and masking algorithm for objects in the FLS Peg Transfer task

Section 2.6: Tool Tracking and Visual Servoing

Tool Tracking

The University of California San Diego (UCSD) focused on developing novel technologies for surgical tool tracking and visual servoing. Figure 9 details their developed surgical perception framework consisting of a deformable tissue tracker and a surgical tool tracker to perceive the entire surgical scene, including the deforming environment and robotic agent. Two deep neural networks are embedded into their framework for specific feature extractions: DNN(1) finds and matches features from stereo images to generate a depth map for tissue tracking, and DNN(2) extracts point features for surgical tool tracking. To track tissue deformations, UCSD updates their tissue model by fusing the estimated depth maps using a previously developed model-free tissue tracker [3]. For their surgical tool tracking, the pose of the tools are estimated using a model-based tracker that utilizes a kinematic prior and fusing the encoder readings with the 2-D detection from the images. To separate the tools from the deformable tissue model, a mask of the surgical tools is generated by rendering the 3-D CAD model into the endoscopic camera view and is removed from the depth map fed to the deformable tissue tracker. Finally, UCSD combines the tissue point cloud and surgical tools into the camera frame to reconstruct the entire surgical scene.

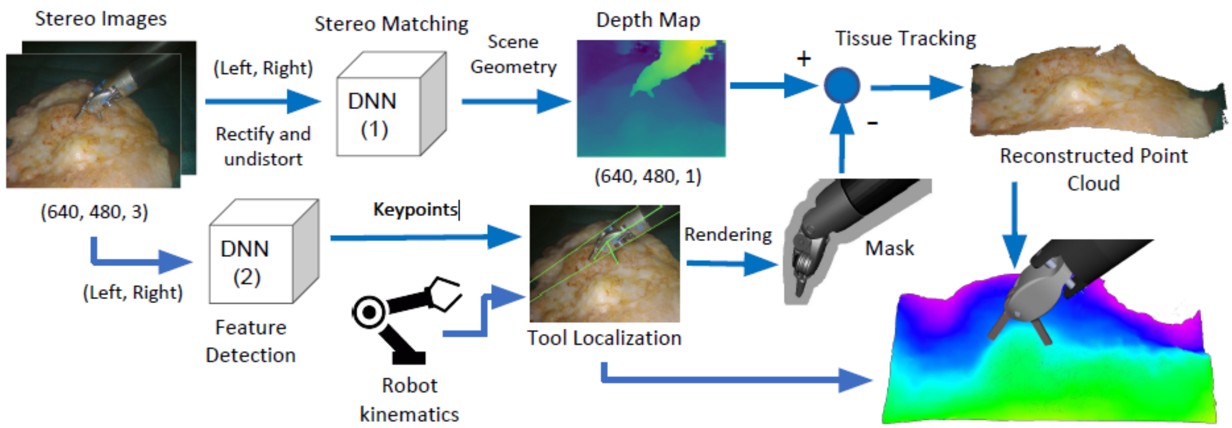

Figure 9: The complete workflow of UCSD's surgical perception framework.

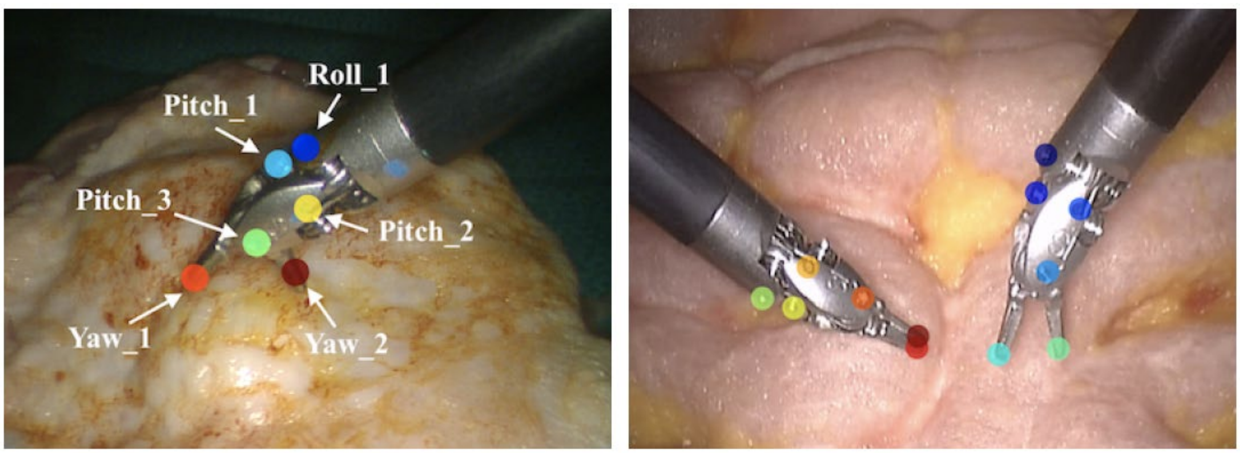

Fig. 10: Illustration of the point features to detect on surgical tools. (Left) the features detected on a single instrument, and (right) the features detected and associated appropriately with two instruments.

Figure 10 illustrates the key points tracked on the tips of the surgical tools. Six locations along the tool tip are tracked and provide important information to the system on the orientation of the tool tip in terms of the tool's roll, pitch, and yaw. To localize the surgical tools UCSD relies on a Deep Neural Network (DNN) model DeepLabCut [4] which uses DeeperCut [5] as the backbone for point feature detection. The DNN consists of variations of Deep Residual Neural Networks (ResNet) for feature extraction and deconvolutional layers to up-sample the feature maps and produce spatial probability densities. The DNN was fine-tuned with few training samples to adapt to surgical tool tracking by minimizing the cross-entropy loss. The samples were hand labeled using the open-source DLC toolbox [6]. Figure 11 shows examples of point features that were detected on surgical instruments. To estimate the pose of the surgical tool in 3-D space, the 2-D detections are combined with the encoder readings from the surgical robot and a particle filter is applied for estimation. To overcome the uncertainties of inaccurate joint angles and challenges of calibrating the transform between the camera and robot base UCSD utilized a previously developed formulation to track the Lumped Error. Lumped Error compensates for both error in joint angles and hand-eye [7].

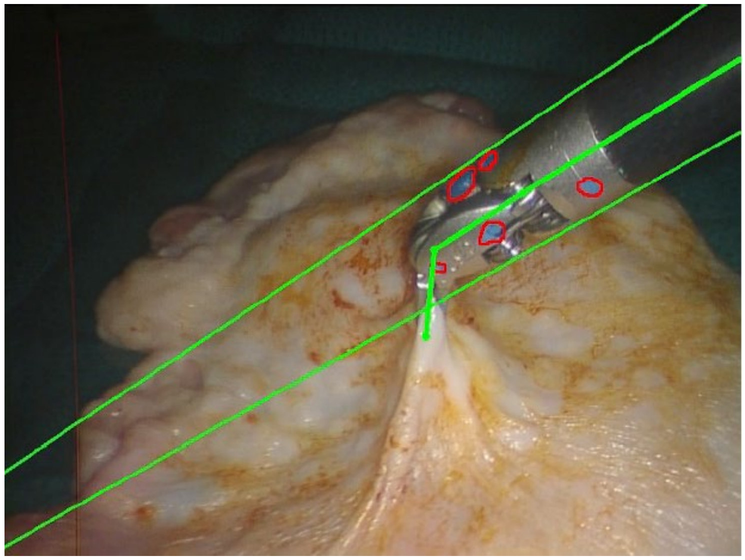

Figure 11. UCSD's surgical tool tracking identifying tool features at the tool tip and angle of the tool shaft.

Suture Tracking

Another focus of UCSD's work during the TRON period of performance was in advancing the state of the art for autonomous suture needle and thread tracking. At the onset of the TRON project the goals for a final demonstration were targeting an autonomous robotic vessel repair or suture demonstration and developing suture tracking perception technologies were paramount to accomplishing that goal under a semi-autonomous framework. The project shifted to a Temporary Vascular Shunt Placement (TVS) procedure late in the project cycle and unfortunately the developed suture tracking technologies were not implemented in the Taurus-M control framework. However, UCSD did win top prize for scientific journal paper in the medical robotics conference at the IEEE International Conference on Robotics and Automation (ICRA) 2023, considered the most prestigious international robotics conference, for their work on suture needle tracking.

To achieve state-of-the-art performance for real-time suture needle tracking in robotic surgery UCSD focused on developing grasping constraints to the position of the suture needle. They developed these constraints to contain the position of the needle logically in a connected position between the grippers of the tool in a position near perpendicular to the grasping prongs. This allowed them to create a probabilistic model on the position of the suture needle. They then developed a state-space to describe a grasped suture needle for efficient sampling on the feasible grasping manifold. Lastly, they created a comparison Bayesian filter approach that would incorporate the grasping constraints. The developed tracking technologies were evaluated in both simulation and real-world environments. UCSD has shown in their experiments that accurately tracking the relative poses is more crucial in successfully automating suture needle manipulation tasks [8].

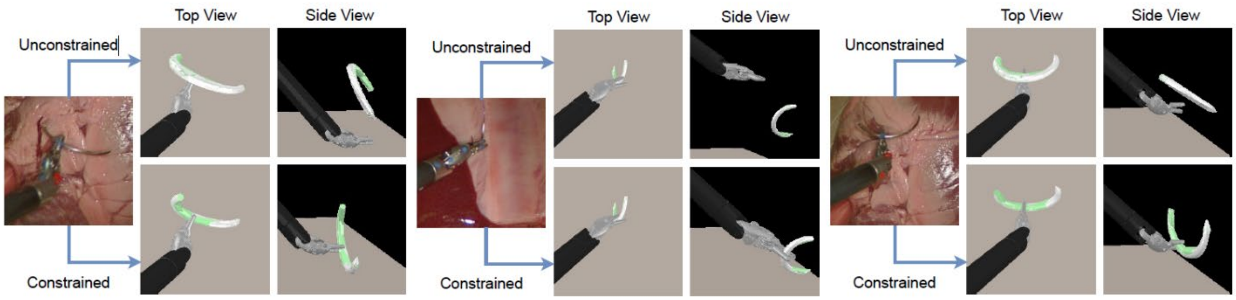

Figure 12 illustrates the methods of tracking suture needles with or without constrained grasping locations and the performance of the tracking in each method.

Section 2.7: Autonomous Robotic Control

Autonomous Framework

The main focus of the University of California Berkely (UCB) was to develop autonomous robotic control routines. They started by using the Da Vinci Research Kit (dVRK) to demonstrate how through depth sensing, certain surgical procedures could be performed autonomously. They published their work in accomplishing the FLS peg transfer task at “super-human” speeds and accuracies, outmatching surgical residents at the task with their autonomous robot control [9]. The research team at UCB successfully demonstrated that highly skilled surgical techniques could be accomplished through advanced autonomous robotic frameworks. UCB used the dVRK surgical robot with a Zivid depth sensor to automate three variants of the peg-transfer task: unilateral, bilateral without handovers, and bilateral with handovers. UCB used 3-D printed fiducial markers with depth sensing and a deep recurrent neural network to improve the precision of the dVRK to less than 1 mm.

From experimental tests with over 1800 peg transfer trials UCB reported that the fully automated system can outperform an experienced human surgical resident, who performs far better than untrained humans, in terms of both speed and success rate. For the most difficult variant of peg transfer (with handovers) UCB compared the performance of the surgical resident with performance of the automated system with over 120 trials each. The experienced surgical resident achieves success rate of 93.2% with mean transfer time of 8.6 seconds. The automated system achieves success rate of 94.1% with a mean transfer time of 8.1 seconds. This is the first fully automated system to achieve “superhuman” performance in both speed and success on the FLS peg transfer task. To make the task even more difficult UCB colored the peg board and triangles all the same hue of red as to not “cheat” with color segmentation and to achieve a more realistic surgical site perception as tissue, blood, and vessels may not be distinguishable by color. They achieved their grasping location based on their depth sensing image processing.

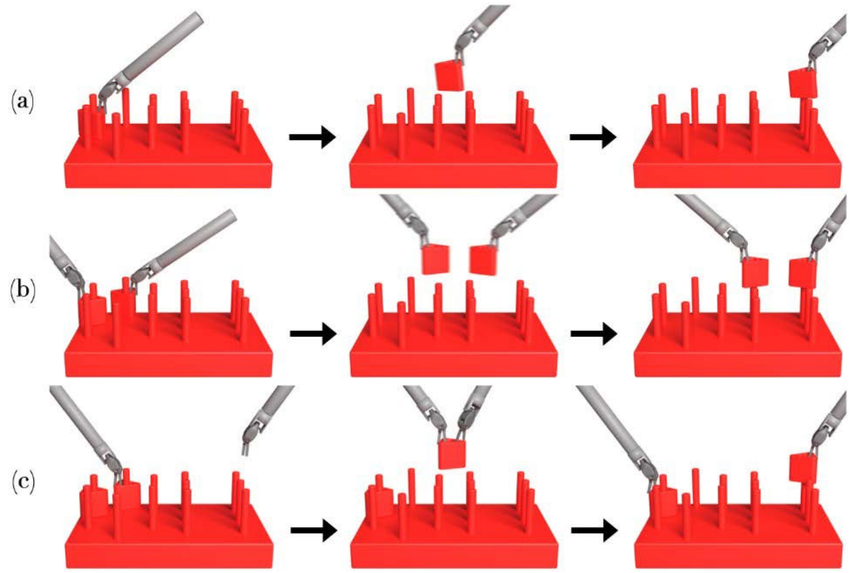

Figure 13. the steps the automated robotic system took to accomplish the FLS peg board task. UCB colored the board, pegs, and triangles red to not rely on color segmentation, making the challenge more similar to live tissue operation.

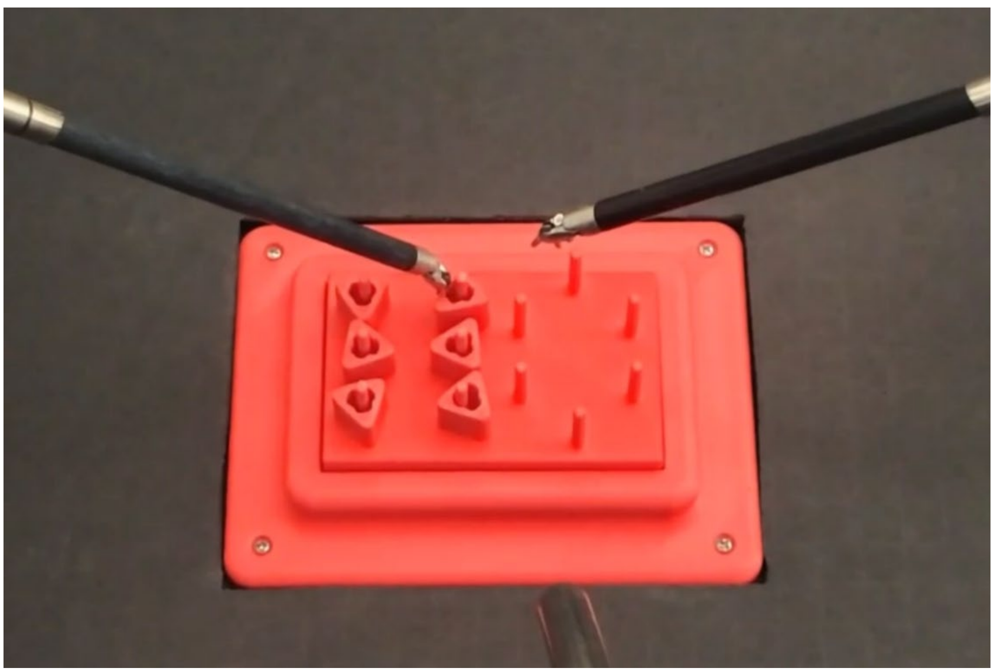

Figure 14. a screenshot of UCB's automated FLS peg transfer task trial.

While the work from UCB was impressive, it was unfortunately unsuccessfully integrated into the Taurus-M controls scheme due to an incompatibility error in the 6 Degree of Freedom (DoF) dVRK system design and the 7 DoF Taurus-M design. SRI had to pivot to an alternative semi-autonomous control framework using a perception technology called OptiTrack.

Adapting Autonomous Control

With the success of UCB's automated FLS peg board trials on the da Vinci Research Kit (dVRK), it was a logical next step to integrate the autonomous control framework into the Taurus-M robot. This proved to be highly challenging as the two robotic systems did not share commonality in their degrees of freedom (DoF). The dVRK is a 6-DoF robot while the Taurus-M is 7-DoF. This difference creates significant integration trouble when trying to map the autonomous robotic control software from one system to the other. This would require two choices, either to start over and redesign UCB's control framework using the Zivid camera on the Taurus-M robot, or pivot to a new autonomous control framework specifically for the Taurus-M. In the end SRI decided to pivot and develop their own semi-autonomous control framework due in part to their doubts in the Zivid depth sensing camera system being the most appropriate for surgical perception. The Zivid camera takes discrete depth sensing images with a bright flash every two seconds and does not allow for continuous tracking. SRI opted to go with the OptiTrack motion tracking camera system for its ability to track fiducial markers continuously at millimeter accuracy.

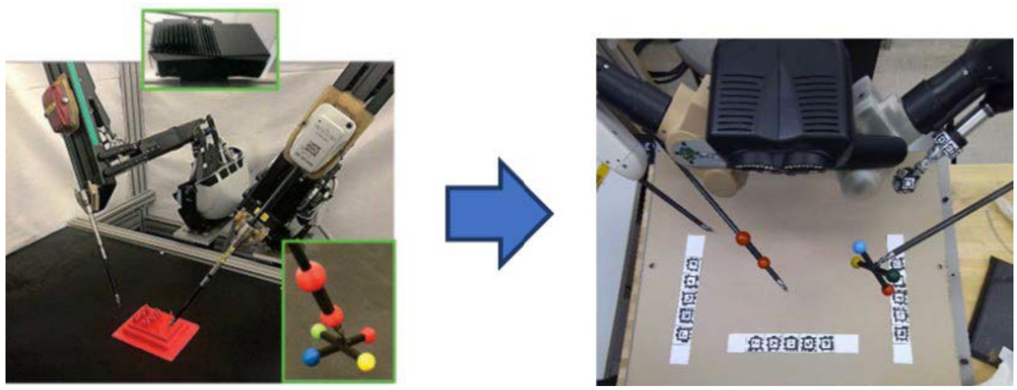

Figure 15. On the left is UCB's dVRK robot with the Zivid depth sensing camera. On the right is SRI's Taurus-M attempting to translate the same control scheme and training.

OptiTrack Sensing

OptiTrack is a system of motion tracking cameras that identify highly reflective fiducials in a scene and can track motion with extreme precision. SRI outfitted the arms of the Taurus-M robot with reflective fiducials and constructed a camera mounting cage around the Taurus-M with five OptiTrack cameras to accurately track and locate the exact position of the robot as it performs surgical tasks. The perception allows for autonomous motion planning once given a high-level surgical task. For the temporary vascular shunt placement procedure, the robot is required to grasp with both hands the edge of a broken vessel and hold it in place for the lead surgeon to insert the shunt. To autonomously locate the grasp points, fiducials were also placed on the tools of the lead surgeon. Once the lead surgeon with their forceps tool grasps the vessel, the robot can track that location to sub-millimeter precision and grasp two other locations on the same vessel.

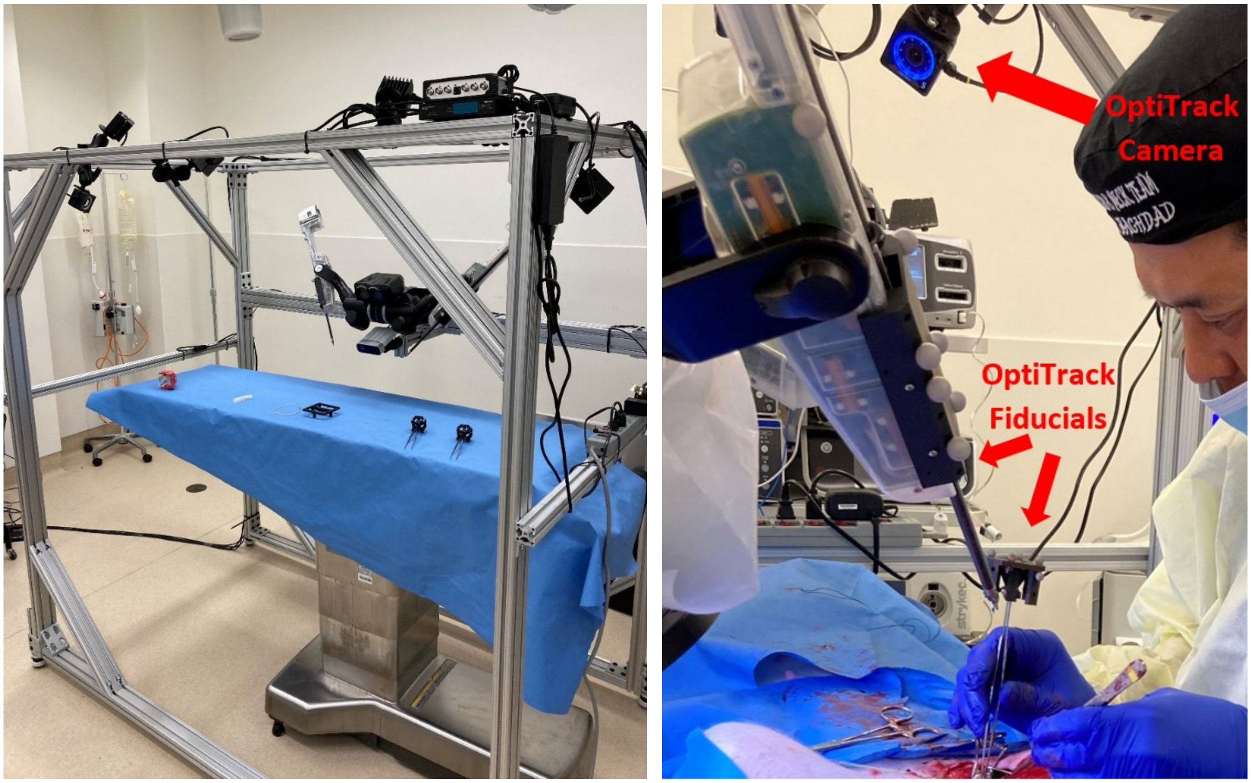

Figure 16. the semi-autonomous Taurus-M framework with OptiTrack cameras and fiducials on the robot arms and surgeon tools.

Vessel Grasp Location

To perform a Temporary Vascular Shunt (TVS) procedure two surgeons need to participate and both grasp the severed vessel. The lead surgeon will grasp the vessel at one end, while the assisting surgeon will then grasp the same vessel at points 120º away from the initial grasp. This allows the three grasp points to maximize the opening created by the surgeons and allow the lead surgeon to then insert a shunt. In the TRON robotic framework, the remote surgeon assisting must grasp the vessel without physically seeing the surgical scene and must rely on the OptiTrack based semi-autonomous framework. Once the lead surgeon grasps the vessel edge with their forceps tool donned with OptiTrack fiducial markers, the remote surgeon is instructed to initiate a grasp command from the robot's Virtual Reality (VR) Operator Control Unit (OCU). The OptiTrack fiducial markers on the surgical forceps allow the TRON system to understand the exact 3-D location and angle of the vessel edge. From there an ellipsoid vessel edge in shape and size is inferred and a calculation takes place to determine where in 3-D space the two other grasps need to be made by the robot.

Intent-Based Semi-Autonomous Control

Semi-Autonomous control for the Taurus-M relies on high-level input from the remote surgeon, however low-level motion planning is handed off to the robot equipped with the OptiTrack high-precision motion tracking capabilities. The high-level control is determined in the remote surgeon's Operator Control Unit (OCU). The OCU is the virtual reality environment that the remote surgeon operates in using an Oculus Rift S headset and hand controllers. Due to the anticipated inoperability of direct teleoperation in high-latency and low-bandwidth of deployed communication environments, the robot does not transmit a video stream of the surgical scene to the remote surgeon, as that would require vast amounts of bandwidth.

Instead, the remote surgeon operates in a simulated digital representation of the surgical procedure, updated by the OptiTrack cameras sensing the surgical scene. This way, only the delta changes in the surgical scene need to be passed over the network to the remote surgeon, greatly reducing the required bandwidth down to kilobytes. Inside the digital simulation of the temporary vascular shunt placement procedure, the remote surgeon sees a simulated vessel and commands the robot to grasp at certain locations along the vessel edge. These high-level commands are then sent across the network and to the robot, allowing it to generate its own path planning to reach the desired grasp locations. By separating high-level commands and low-level motion planning, the latency in the network does not lead to errors. This is achieved because despite seconds of latency in the network between the remote surgeon issuing a high-level command, the actual motions of the robot are generated and controlled in real-time at the surgical site through the closed-loop autonomous movement control of the OptiTrack system. If the robot can still identify the edges of the vessel, it can carry out the grasps autonomously.

To address the challenges posed by extreme network latency that renders teleoperation impractical, we have developed an innovative semi-autonomous control strategy. This strategy, intent-driven control, compensates for the significant limitations imposed by the network and ensures effective execution of remote surgical procedures. The remote surgeon provides high-level surgical decisions, and the robot carries out low-level motion planning to accomplish the commands autonomously. This intent-based control approach enables the robot to calculate path planning for each motion command, minimizing the risks of overshoot and collisions commonly found in high-latency teleoperation. By breaking down the surgery into small sub-steps or "surgemes," the robot can perform simple motion commands without the need for advanced intelligence on full surgical procedures or clinical decision-making. The remote surgeon transmits commands on where to grasp, cut, or puncture, which the robot interprets using its perception technologies to carry out low-level motion planning, virtually eliminating latency as a source of error. Fig. 20 illustrates the control process flow diagram for the intent-based control strategy.

Latency can be mitigated by sending high-level landmark-based commands to the robot. For example, if the surgeon's intent is to use the robot's right arm to hold the lip of a severed artery at the point closest to the surgeon, then a message to "grip artery at the closest point to the camera using the left-side gripper" can be sent from the operator to the robot. This approach requires sensing and intelligence on the robot that:

1) Identifies the artery's severed end in the robot's visual field
2) Understands the spatial relationship between the artery's severed end and the camera
3) Can compute the location of the point closest to the camera
4) Understands which robot arm is the "left" arm
5) Can move to and grip the correct point on the artery's lip (or report back that the command cannot be completed).

This approach, one that uses high-level, landmark-based messages, has several advantages. First, the commands can be infrequent and brief, thus requiring less bandwidth than low-level streams of commanded state updates. Second, they accommodate changes in the surgical site's state. In the example above, if the artery moves in relation to the robot, the robot can track the artery locally and grip it at the point closest to the camera even though the artery is not in the same position it was when the operator issued the command. Once it has gripped the vessel, it sends an update back to the operator's console and the simulation on the console can show the robot's left gripper holding the artery.

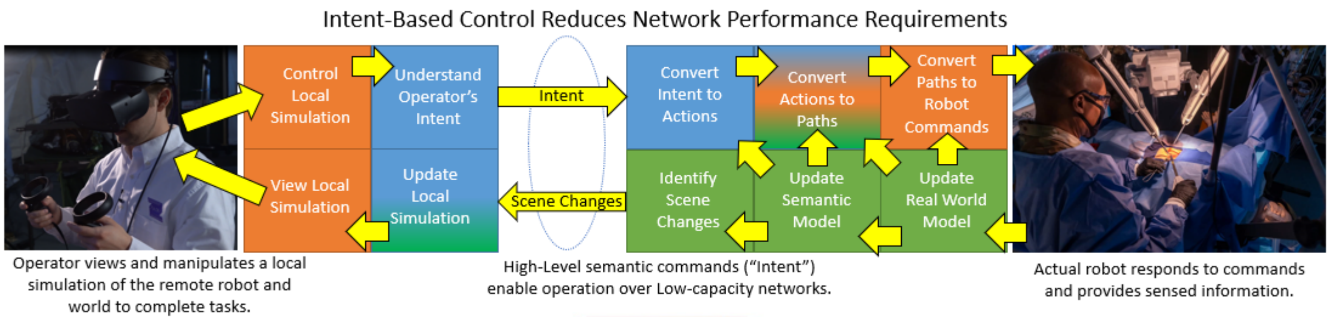

Figure 17. system diagram of "intent-based" semi-autonomous robotic control.

Live Animal Study

Section 3.1: Temporary Vascular Shunt Placement Procedure

Relevance

The Temporary Vascular Shunt (TVS) replacement procedure is employed as a medical intervention to manage arterial trauma affecting the extremities when specialized vascular surgery facilities are unavailable. A TVS procedure was chosen for our capstone proof-of-concept demonstration because it is operationally relevant as a commonly used solution to battlefield trauma injuries. The location of when a TVS procedure would be conducted also fits the possible deployment of the Taurus-M robot. A TVS typically would be conducted at a Forward Surgical Team or Role 2 facility where there are surgeons but not vascular specialists to fully repair the vessel. A TVS procedure can buy the patient more time before further evacuation to larger Role 3/4 facilities.

A TVS procedure involves creating an artificial connection between an artery and vein to restore their functionality, providing temporary stabilization until the patient can receive definitive treatment in a hospital setting. This technique redirects blood flow, ensuring oxygenated blood reaches the affected area, preserving tissue viability, and minimizing the risk of complications such as ischemia or tissue necrosis. In Fig. 18, the vascular shunt replacement procedure is depicted on the left hind leg artery of a large swine test subject. The vascular shunt technique has proven to be a valuable interim measure, offering a lifeline to patients in urgent need of vascular intervention in extreme environments where immediate specialized surgical options are not readily available.

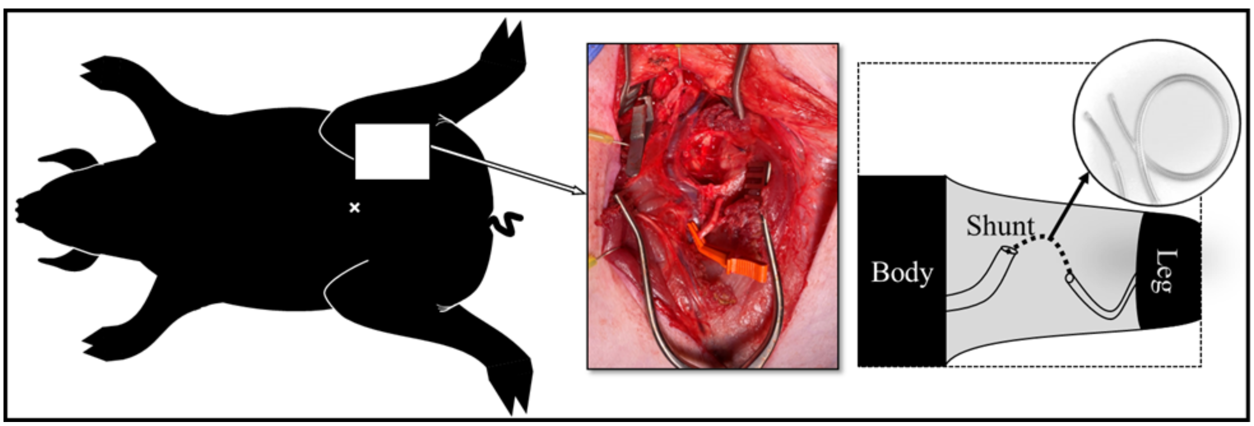

Figure 18. A diagram showing the location on the pig where the femoral artery would be severed and temporarily repaired through a temporary vascular shunt placement procedure.

Procedure

We conducted a live animal study to investigate the potential application of the Taurus-M surgical robot as a supportive tool for temporary vascular shunt placement for femoral artery in pigs. Our study design follows our approved Institutional Animal Care and Use Committee (IACUC) protocol #S22126 submitted to the University of California San Diego. The study comprises two test sets: teleoperation and semi-autonomous procedures with varied network latency. The teleoperation test is designed to demonstrate the feasible network latency level for successful teleoperation in vascular shunt procedures by introducing a range of artificial network latency. Under the assumption of extreme network conditions characterized by significantly higher latency that yields teleoperation infeasible, we assess the efficacy of the intent-based control strategy in the semi-autonomous framework for operating the robot and achieving successful shunt placement. The success of the procedure is determined by confirming positive flow across the vascular shunt using a Doppler flow probe. The time taken to complete the procedure is recorded for every procedure. To evaluate the impact of network latency on the performance of the robot, we simulated varying levels of network latency, ranging from 250ms to 1,000ms for teleoperation and 6,000ms for semi-autonomous control. The subsequent subsections detail the results of the animal study, including scientific findings and insights gained during the animal study. For the experiments, we utilized 3 pig samples, each with an approximate height of 160cm and a weight of 70-100kg, and employed medical shunts manufactured by Integra Lifesciences, Princeton, NJ. Fig. 25 shows an animal study conducted in the operating room, where the Taurus-M telesurgical robot platform is utilized for vascular shunt replacement procedures.

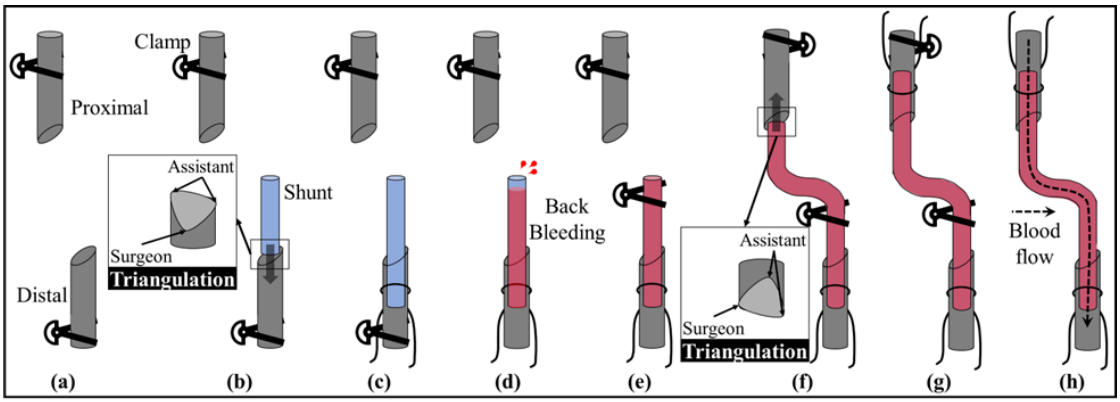

Figure 19. the steps to complete a Temporary Vascular Shunt Placement (TVS) procedure.

Step 1. (Preparation) Clamp the two ends of the artery (a).

Step 2. Grip three spots of the opening of distal artery to make “Triangulate” the opening (b).

* Two vertices by assistant and one vertex by lead surgeon

Step 3. Insert shunt about 2 cm into the distal artery (b).

* Assistant: Hold the distal artery in place

Step 4. Tie the knot around the distal shunt and artery (c).

Step 5. Release clamp on the distal artery to back bleed removing all air in the shunt (d).

Step 6. Clamp the middle of the shunt to stop the blood flow (e).

Step 7. Create triangle opening on the proximal artery (Samp procedure to Step 2) (f).

Step 8. Insert the shunt into the proximal artery about 2 cm (f).

* Assistant: Hold proximal artery in place

Step 9. Tie the knot around the proximal shunt and artery (g).

Step 10. Release the clamps on both the proximal artery and the middle of the shunt (h).

Figure 20. the steps to complete a Temporary Vascular Shunt Placement (TVS) procedure.

Section 3.2: Robotic Assistance for Shunt Procedure

Operator Control Unit Simulation

Figure 21 below shows a representation of the surgical site suitable for sending commands to the robot. The figure shows the location where the attending surgeon gripped the vessel with forceps. The OCU-side surgeon grips the vessel with one of the simulated robot's grippers (not shown). Once the gripper holds the vessel, the simulator's software computes the grip location relative to the forceps grip location and sends the relative location to the robot. Software on the robot converts the incoming angle, relative to the forceps, into a pose relative to where the forceps are gripping the physical vessel and then commands the robot to move the correct gripper to that location and close the gripper.

Figure 21. the digital representation of the vessels in the remote operator's OCU.

Tracking Surgeon Tools

Fiducial markers on the lead surgeon's forceps tool provided a tracking apparatus for the TRON system. The OptiTrack cameras mounted on the robot cage surrounding the surgical bed not only track the robot's arms but also the surgeon's tools. The exact 3-D location of the surgeon's tools begins the calculation of where the TRON system understands the location of the desired vessel is and allows for the calculation of the remaining two grasp points. The orientation of the surgeon's tools plays an important role in signaling to the remote surgeon when to initiate a robotic grasp. If the surgeon is holding their tools in a vertical position, then the TRON system displays the forceps as a transparent representation in the remote surgeon's OCU. The fiducials are also asymmetric so the direction the surgeon is facing the tools also indicates to the TRON system if the lead surgeon is gripping on the far or close edge of the vessel relative to the Taurus-M robot. The lead surgeon will only position their tools vertically when they have successfully grasped the vessel and will place the tools down horizontally on the bed at all other moments. This provides an autonomous indication to the remote surgeon on the activity of the lead surgeon.

Figure 22. the lead surgeon grasping the edge of the damaged vessel with forceps topped with OptiTrack fiducials. With the surgeon's tools in a vertical position, the TRON system alerts the remote surgeon to initiate the next grasping motions.

Section 3.3: Study Preparation

In-Lab Tests

TATRC conducted multiple in-lab trials of the TVS procedure using the Taurus-M robot and synthetic tissue. In-lab tests allowed for both procedural practice for the robotic surgeons as well as data gathering opportunities using TATRC's Taurus-M robot. Depth imaging data during trails of TVS procedures were provided to the University of Chicago as datasets to train their vessel detection computer vision algorithms. The in-lab trials also provided vital insight into the procedure for information required for the IACUC protocol regarding procedural steps in the novel configuration of a surgeon being assisted by a teleoperated surgical assist robot.

Figure 23. the lab set up of TATRC's Taurus-M surgical assist robot practicing TVS procedures.

Animal Lab Setup

The first two days of the four-day animal study involved configuration setup of the two Taurus-M robots and calibration. TATRC shipped the directly teleoperated version of the Taurus-M used for the trials without autonomy. This robot simply required its base stand to be rebuilt on site and system checkouts were conducted. SRI brought with them to the animal study their Taurus-M which was configured for semi-autonomous control. Around SRI's robot a camera cage needed to be assembled to house the OptiTrack cameras which provide the tracking feedback necessary for the semi-autonomous control framework. Once built, the OptiTrack system required calibration. A series of practice trials were conducted using both robots on synthetic tissue similar to the in-lab trials conducted at TATRC to ensure both robots were ready for the remaining two days' animal procedures.

Figure 24. TATRC's Taurus-M surgical assist robot configured for direct teleoperation control

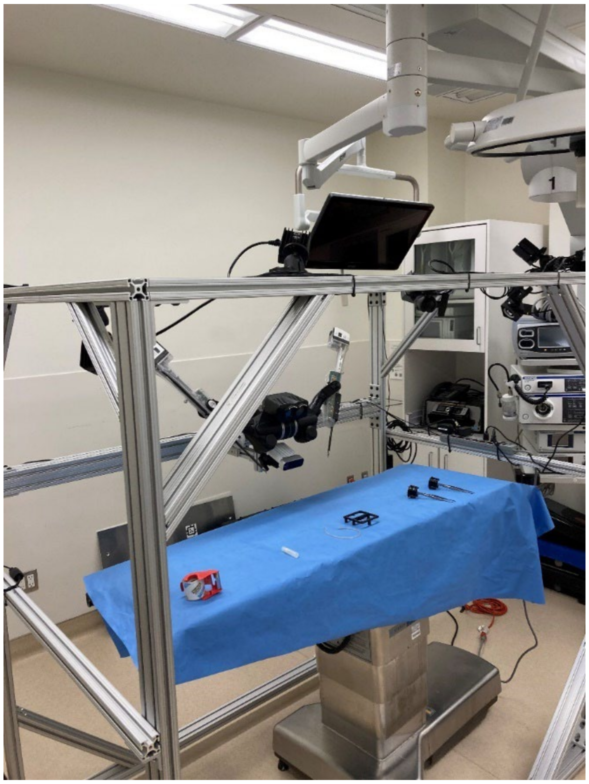

Figure 25. SRI's Taurus-M surgical assist robot configured for semi-autonomous control.

In the final steps of preparation both robots were covered with plastic surgical drapes to sterilize and waterproof the systems from the possibility of squirted blood from the highly pressurized femoral artery. The Taurus-M system in its current iteration does not have inherent waterproofing and required drapes.

Figure 26. the directly teleoperated version of the Taurus-M in surgical drapes for waterproofing and sterilization.

Section 3.4: Study Execution

Two Surgeon Control

Prior to initiating robot-assisted surgery, we conducted 12 tests involving two skilled human surgeons to evaluate the general procedure as crucial ground truth tests. The average total procedure time was determined to be 106.47 seconds, with a standard deviation of 50.18 seconds, indicating variability in the time required for the procedure. The duration of the tests varied depending on the individual surgeons and the initial time required for them to become acquainted with the trials. Note that the test is processed with two of three surgeons who are rotationally selected. During the tests, we observed the occurrence of errors, typically resulting from simple mistakes that are commonly encountered. Specifically, out of the 12 tests conducted, a total of 4 errors were observed. These errors mainly resulted from minor mistakes, such as shunt slippage during insertion and challenges in knot tying due to the limited workspace relative to the size of human hands. However, it is important to note that these errors had minimal impact on the overall procedure time, except for the first test where the errors slightly extended the duration due to the surgeons' initial adjustment period to the procedures. Overall, these findings provide valuable insights into the procedure and serve as a reference for comparisons with robot-assisted procedures.

Teleoperation Nominal Latency

The first robot-assisted procedure involved teleoperation control, with and without network latency, and the results were analyzed. Tests without latency demonstrated promising outcomes, with an average processing time of 181.60 seconds under ideal network conditions. Although slightly longer than the time taken by two human surgeons, the smaller standard deviation indicated less variation compared to human procedures. The average robot assistance time was 94.86 seconds, with a standard deviation of 20.66 seconds. Part of the time can be attributed to performing general robot operating functions, such as camera zooming and clutch activation for long-distance translations. Errors arising from non-critical human errors, robot operations that resembled common errors seen in human procedures (e.g., missed grips, incorrect grips, or slips), and certain functional problems with the robot, such as a camera zoom failure, contributed to the increasing error rates. The challenge of grasping vessel openings was reported by robot pilots due to color similarities, affecting depth perception in the remote VR view. Despite these limitations, the teleoperation tests showed promise, with an average error rate of 1.44 and only 2 trials experiencing a maximum of 3 errors. Overall, teleoperation demonstrated potential when compared to procedures performed by two human surgeons, despite the slight increase in processing time due to robot operations.

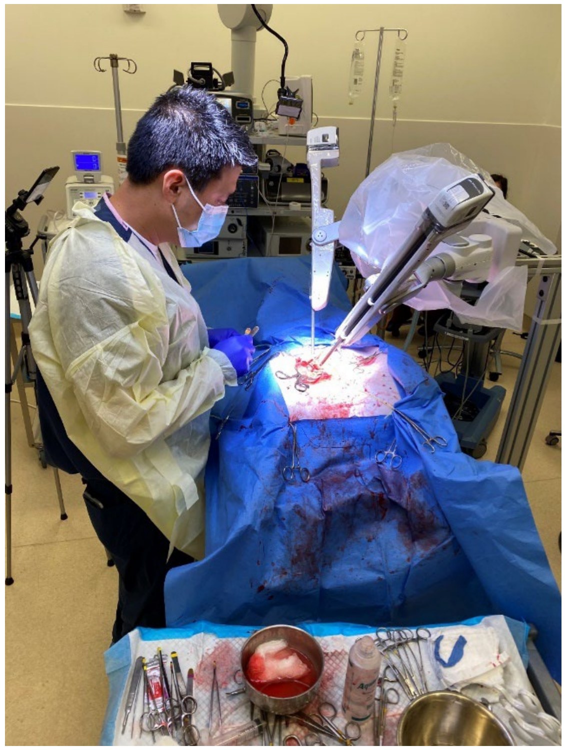

Figure 27. live animal study TVS procedure with the Taurus-M robot directly teleoperated.

Teleoperation Inserted Latency

In the subsequent test, telerobotic assistance was evaluated with different levels of latency. The test involved latency durations of 0ms, 250ms, 500ms, 750ms, 1,000ms, and 3,000ms, randomly assigned for each procedure without prior notification to the robot operators. The average procedure time was 216.07 seconds, with a standard deviation of 60.69 seconds, while the average robot operation time was 131.92 seconds, with a standard deviation of 60.47 seconds. The network latency presents challenges for operators in accurately controlling the robot, particularly in tasks that involve close interaction between the human surgeon and the robot. This is due to the unavailability of immediate and precise reactions, which is essential for tasks involving the maneuvering of the robot arm based on the surgeon's instructions. However, measuring the precise impact of latency levels below 1,000ms on procedure time is challenging. Despite the general trend of increased overall procedure time due to added latency, determining the exact influence of latency level becomes difficult as the total processing time tends to vary randomly in such cases. Notably, a clear trend was observed with longer procedure time in tests with a 3,000ms latency. During the 18 trials with random latency, both the human surgeon and the robot observed common errors such as missed grips, slips, or shunt slippage. Despite the extended processing time, the error rates remained consistent, and the types of errors encountered did not create significant obstacles in completing the procedure, as they were similar to those observed in latency-free experiments. The tests have shown that robot-assisted vascular shunt procedures can be performed remotely despite network latency fluctuations. The extended processing time is deemed acceptable, allowing for surgical operations in demanding network environments.

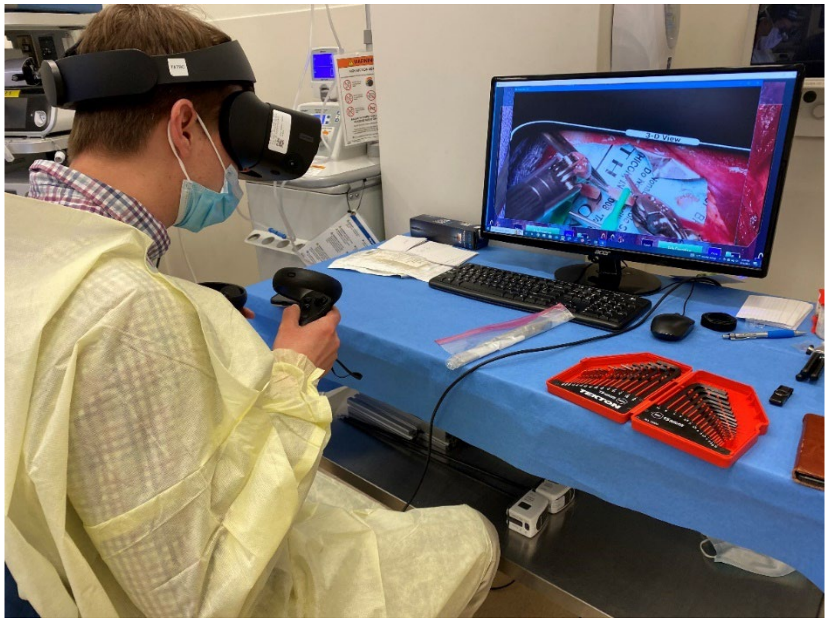

Figure 28. the remote surgeon operating the VR Operator Control Unit to teleoperate the Taurus-M robot during the live animal study. While physically in the operating room, simulated latency was inserted into the network.

Semi-Autonomous Control Under High Latency

During the teleoperation with latency tests, it was observed that when the network latency reached 3,000ms, the remote robot assistance procedure encountered increased processing times and a higher error rate. To address this issue, we also tested out our developed semi-autonomous control framework. We conducted tests comparing vascular shunt procedures with and without high network latency (0ms and 6,000ms). The presence of high latency did not show a definitive connection between the overall completion time of the procedure and the duration of robot operation or the occurrence of errors in the semi-autonomous control mode. As a result, it can be concluded that the semi-autonomous algorithm utilizing intent-based control was either less impacted or unaffected by highly delayed control signals, as long as the shunt procedure was executed accurately and in the correct sequence. Despite resulting in a longer total procedure time, the implementation of the semi-autonomous control effectively addresses significant latency issues. The increased time is primarily attributed to the slower robot operation associated with the early-stage testing of the algorithm. However, this limitation can be improved in the future. Moreover, it is meaningful that the error rate, averaging at 0.81 with a standard deviation of 0.75, was lower compared to previous tests and mainly consisted of common types of mistakes. Despite the extended processing time, the reduced error rate renders the system suitable for demanding application scenarios characterized by high latency in remote robotic assistance.

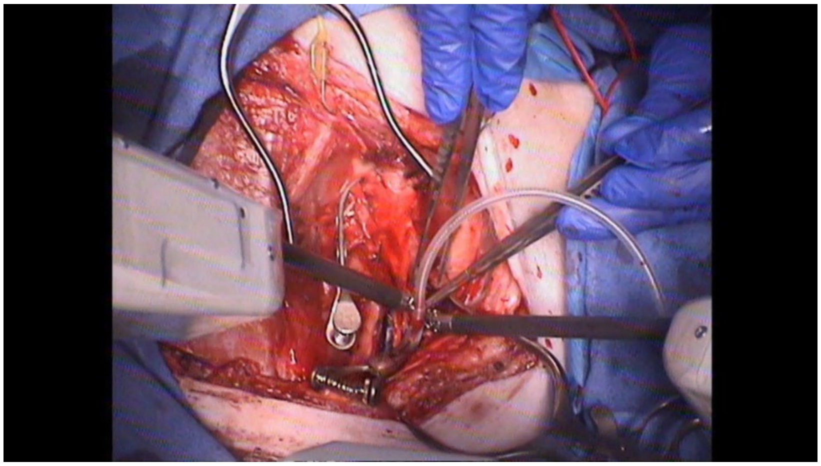

Figure 29. a overhead view of the TVS placement procedure during the live animal study.

Figure 30. the remote surgeon operating the semi-autonomous framework during the live animal study.

Section 3.5: Results

Procedure Success

During the animal study video of each procedure was recorded from 3 points of view. Two cameras stationed on tripods on opposite sides of the surgical bed provided views of the surgeon, robot, and surgical site. A "skycam" camera integrated into the overhead surgical lights installed in the operating room also provided a top-down view directly into the surgical site. These recorded views of each procedure allowed for accurate analysis and review of each procedure to determine and confirm our primary metric of success, patency across the shunt, and our secondary metrics of success, time to completion and surgical errors.

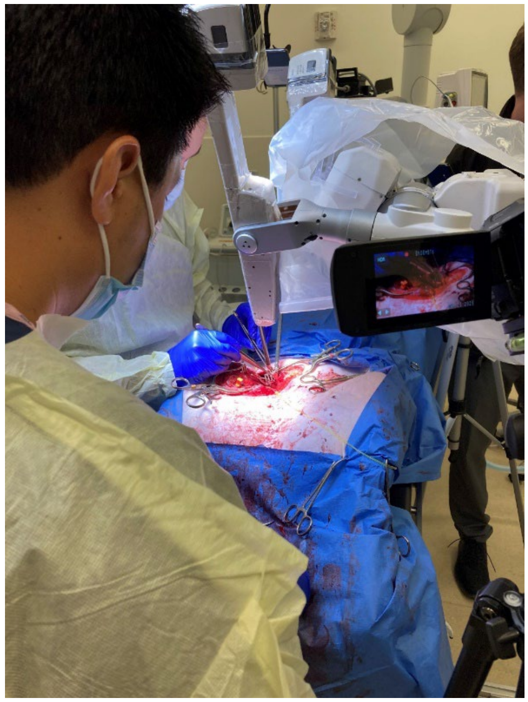

Figure 31. video recordings were captured of each procedure trial during the animal study.

In a total of 55 total procedures, only one did not result in a success of blood flow across the shunt. The single failure came from the first procedure conducted by the control team of two lead surgeons. The failure was a result of blood clotting along the shunt and was later remedied during the second procedure by the injection of heparin into the vessel and shunt before use. Use of heparin in vascular repair surgeries has been suggested from the Joint Trauma System's Clinical Practice Guidelines for vascular injuries [23]. After the first control trail, the remaining 54 subsequent trials all resulted in a successful measure of blood flow across the shunt, as measured by Doppler confirmation on the distal vessel. This included a 100% success rate of 36 trials run with the Taurus-M robot involved. We found through our study that regardless of latency or control framework the Taurus-M robot was always successfully able to assist the surgeon in performing this procedure.

Time to Completion

Time to completion was defined as the time between the initial grasp of the proximal vessel by the lead surgeon and the moment the Doppler device successfully confirmed flow at the distal vessel. Results from this secondary metric of time confirmed our initial hypothesis that time would increase through robotic control and even more in semi-autonomous robotic framework compared to two humans. Interesting to note was that time did not vary much depending on the inserted latency and most interestingly is that time-to-completion decreased when latency was inserted into the semi-autonomous trials. We believe this is due to two main factors, we did not conduct enough trials at each study group to find statistically relevant data regarding time differences, and a learning bias. We performed the inserted latency trials after the direct teleoperated and zero-latency semi-autonomous trials. It was seen consistently that the first few trials with the robotic control took longer than later trials as a learning bias was active on how quickly the procedure could be performed. Future studies will ensure that both effects are diminished by conducting a statistically relevant number of trials per study group and randomizing the order of the trials.

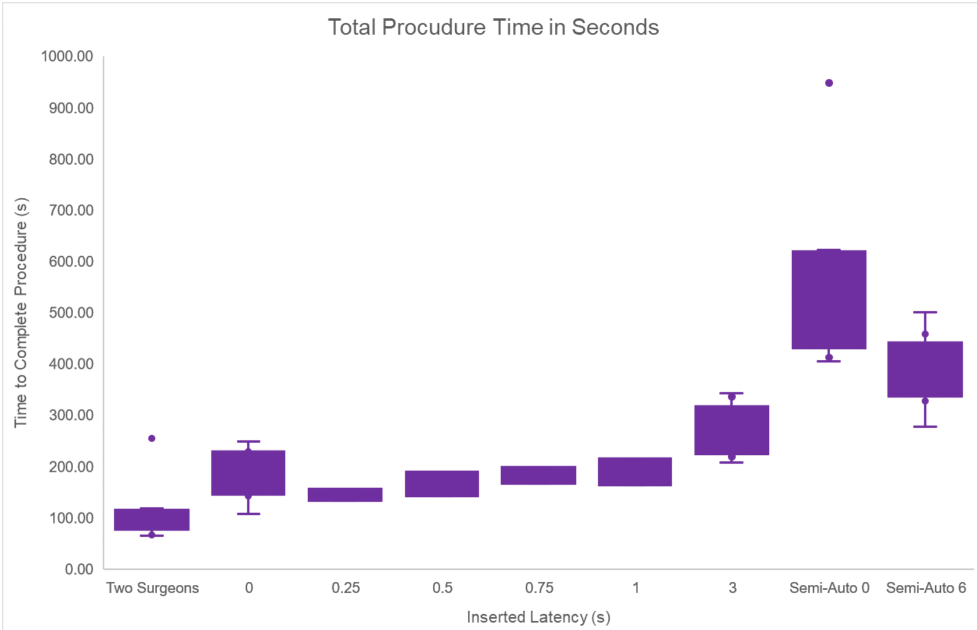

Figure 32. data gathered during the animal study on the time to complete a TVS placement procedure between the different inserted latency study groups.

Surgical Errors

Surgical errors were defined as slips of the vessel grasp, missed grasps by under or overshooting the vessel, slips of the knot off the vessel, and incorrect knot ties. Measured errors consisted of both the lead surgeon and the robot. Once again it is important to note that we did not conduct enough trials per study group to have statistical relevance on our measurement of errors. One interesting insight from the data is that errors did not drastically increase when latency was inserted, and similarly to time-to-completion, the semi-autonomous framework improved performance despite six seconds of latency in the network. This does demonstrate a strong case that the semi-autonomous framework could possibly be a safe method for employing surgical assistance across far distances with intermittent and latent communication.

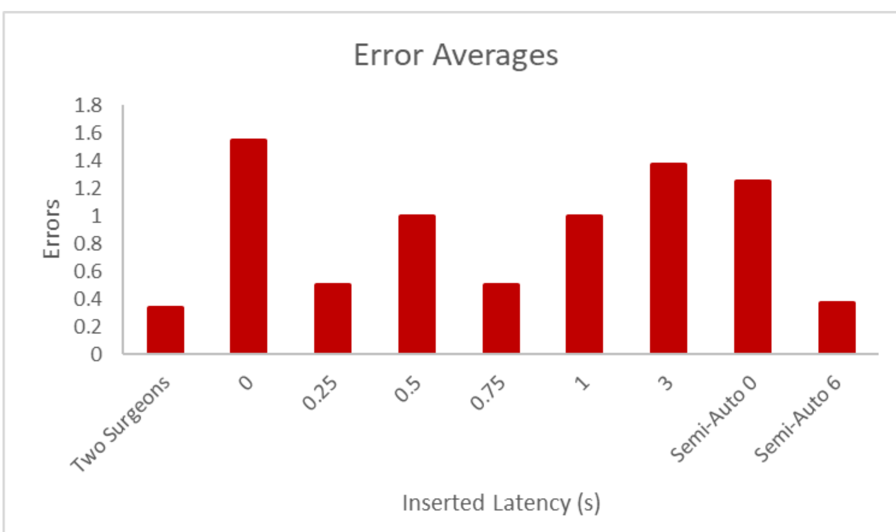

Figure 33. data gathered during the animal study on the average errors of a TVS placement procedure between the different inserted latency study groups.

Section 3.6: Discussion

Discussion

We conducted 55 live porcine tests to evaluate the effectiveness of vascular shunt replacement procedures using the novel surgical robot platform. The target surgery area was the left or right femoral artery of the hind leg of each pig. The first test served as a reference and involved two professional surgeons performing the shunt replacement procedure. In the second and third test groups, one surgeon was assisted by the remote or semi-autonomous robot system. We compared the second and third test groups with the first group to assess the performance of the developed robotic assistance. In the second test group, the robot was teleoperated assuming relatively small network latency (≤1,000ms). The third test group focused on validating the semi-autonomous features of the robot platform, assuming higher network latency (6,000ms). Most tests, including those performed by two surgeons, showed common errors in the vascular shunt procedures, such as missing, slipping, and knotting the shunts properly. The robotic assistance procedures did not introduce any critical errors beyond robot system malfunctions compared to the two surgeons' procedures. Despite observing slightly higher error rates during robot-assisted procedures, distinguishing errors between multiple robot operating modes and different latencies was not clear. Notably, the semi-autonomous procedure exhibited the lowest error rates compared to any robot-assisted procedures. The introduction of latency during teleoperation tends to have an impact on processing time, although the relationship between latency and processing time was not clearly definitive. In the case of semi-autonomous procedures, the processing time was higher, but latency did not have a significant effect on the procedure times. Although the robot-assisted procedures took longer than the two surgeons' procedures, our findings suggest that our novel telerobotic surgical system can effectively overcome network latency and provide satisfactory performance in collaboration with human surgeons for vascular shunt procedures. These promising results highlight the viability of our robot platform for remote operations in emergency trauma treatment. Ultimately, the ability to perform critical procedures remotely under the guidance of expert surgeons through our robotic platform holds great promise for effectively managing and treating trauma casualties in emergency settings. The success of our semi-autonomous robotic control framework also provides the opportunity to assist in remote surgery at distances otherwise completely impossible through direct teleoperation. For reference the six seconds of latency we tested during our live animal study, all of which were successful, is representative of three times the observed latency from the Earth to the Moon.

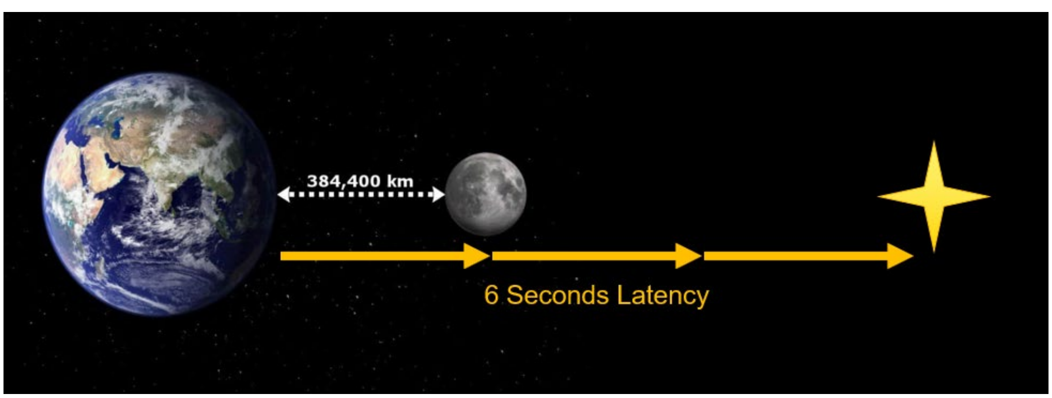

Figure 34. representation of the observed latency distance we tested during our live animal study of a robotic system assisting a surgical procedure using our semi-autonomous framework.

In the future, we anticipate conducting additional studies to validate the capabilities of our innovative telesurgical robot platform in various potential surgeries. We will focus on enhancing the stability and speed of the semi-autonomous control algorithm, while also implementing intelligent motion planning. These advancements are crucial to ensure the feasibility and reliability of autonomous operations. Our research will also involve exploring AI and vision-based surgical scene recognitions, such as identifying surgical tools, tissues, organs, and vessels during the surgery. This integration will enable further automation and facilitate stable interaction with local human surgeons. Additionally, we plan to modify the hardware to create a wider and more efficient workspace for more broader target surgeries. In addition, our future works involve preparing the existing system along with its associated documentation, as well as the test and analysis results, to obtain FDA approval.

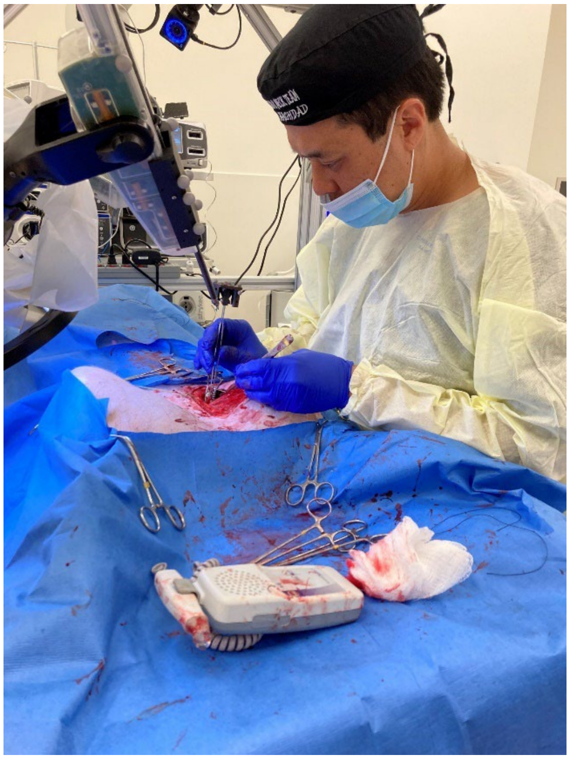

Figure 35. the Taurus-M robot assisting a surgeon perform a TVS procedure during the live animal study using the developed semi-autonomous robotic control framework.

Conclusion

Project Accomplishments

Over the course of the four-year research effort for the TRON project the team developed and manufactured three prototype telesurgical assist Taurus-M robots and delivered them to TATRC and the United States Army Institute for Surgical Research (USAISR). The team designed and implemented a novel semi-autonomous robotic control framework and proved its safety and efficacy in an IACUC approved proof-of-concept animal study under high latency conditions relevant to geographic distant teleoperation. Between TATRC, SRI, The University of California San Diego, The University of California Berkeley, and The University of Chicago, fourteen scientific journals [10-22] were published in clinical and IEEE scientific journals. One paper "Real-Time Constrained 6D Object-Pose Tracking of an In-Hand Suture Needle for Minimally Invasive Robotic Surgery" by UCSD won best paper for Outstanding Healthcare and Medical Robotics at IEEE Conference for Robotics and Automation, arguably the most prestigious conference in the robotics field.

Most importantly this project provides a foundational research platform for the United States Army for further investigation of teleoperated and autonomous robotic-assisted surgery by developing a prototype robotic system that is ideal for future and continued research. The Taurus-M platform is designed to be lightweight, portable, and easy to use with its small footprint and quick set up. The Taurus-M is an ideal robotic platform to continue research into surgical automation, ideal tasking for surgical assistance, and effects of signal latency and disturbance on surgical teleoperation. Since the robot has modular tool adapters, a wide array of possible surgeries and assistive tasks can be investigated.

Fig 36. the Taurus-M surgical assist robot assisting a surgeon in a demonstration procedure in a simulated Role 2.

Next Steps

The TRON project is continuing through a follow-on three-year effort titled Telesurgical Robotic Operative Network for Surgical Assist (TRON-SA). In this research effort we will be focusing on advancing the direct teleoperated control framework while leaving the autonomy aspects for other projects and research opportunities. The reason we chose to focus on the direct teleoperation is due to the advancements in 5G communication, making direct teleoperate more feasible, as well as the technology's maturity and more near-term possible adoption than autonomous frameworks.

One major assumption the TRON animal studies had was the nature of the inserted network latency being a static delay in signal. In real-world networks across geographic distances the signal delay in variable and bounces between a high and low network delay mark. This creates a jitter and inconsistent delay that makes teleoperation of surgical tools much more difficult than through static latency which can be adapted to more easily by the human brain. In TRON-SA we intend to test under real-world dynamic latency and develop novel latency mitigating techniques to enhance the ability for teleoperation. One technique we will be investigating is Adaptive Motion Scaling which will adjust the ratio of operator movement input to robotic movement output based on the perceived network signal latency. This will create smaller robotic movements when the signal latency spikes higher, hopefully diminishing the negative outcomes of overshoot and collisions. We will be concluding the TRON-SA research effort in a robust non-inferiority study between the standard of care two surgeon teams vs teams consisting of one local surgeon and one remote surgeon operating the Taurus-M robot. The study will be conducted on live porcine models during both a temporary vascular shunt placement procedure as well as a microvascular anastomosis procedure.

Figure 37. the Taurus-M assisting a microvascular anastomosis procedure in preliminary lab trials

References

[1] U.S. Army Medical Department. *Memorandum: U.S. Army Medical Department's Position for the Employment of Robotic and Autonomous Systems in Support of Combat Casualty Care, Casualty Evacuation, and Medical Logistics in Army Health Support Operations.* 2018.

[2] Orosco, Ryan K., et al. “Compensatory motion scaling for time-delayed robotic surgery.” *Surgical Endoscopy*, vol. 35, no. 6, 2020, pp. 2613–2618, https://doi.org/10.1007/s00464-020-07681-7.

[3] Y. Li, F. Richter, J. Lu, E. K. Funk, R. K. Orosco, J. Zhu, and M. C. Yip, “Super: A surgical perception framework for endoscopic tissue manipulation with surgical robotics,” IEEE Robotics and Automation Letters, vol. 5, pp. 2294–2301, April 2020.

[4] A. Mathis, P. Mamidanna, K. M. Cury, T. Abe, V. N. Murthy, M. W. Mathis, and M. Bethge, “Deeplabcut: markerless pose estimation of user-defined body parts with deep learning,” Nature neuroscience, vol. 21, no. 9, p. 1281, 2018.

[5] E. Insafutdinov, L. Pishchulin, B. Andres, M. Andriluka, and B. Schiele, “Deepercut: A deeper, stronger, and faster multi-person pose estimation model,” K. He, X. Zhang, S. Ren, and J. Sun, “Deep residual learning for image recognition,” 2015.

[6] T. Nath, A. Mathis, A. C. Chen, A. Patel, M. Bethge, and M. W. Mathis, “Using deeplabcut for 3d markerless pose estimation across species and behaviors,” Nature Protocols, 2019.

[7] F. Richter, J. Lu, R. K. Orosco, and M. C. Yip, “Robotic tool tracking under partially visible kinematic chain: A unified approach,” arXiv preprint arXiv:2102.06235, 2021.

[8] Chiu, Zih-Yun, et al. “Real-time constrained 6d object-pose tracking of an in-hand suture needle for minimally invasive robotic surgery.” *2023 IEEE International Conference on Robotics and Automation (ICRA)*, 2023, https://doi.org/10.1109/icra48891.2023.10161291.

[9] Hwang, Minho, et al. “Automating surgical peg transfer: Calibration with deep learning can exceed speed, accuracy, and consistency of humans.” *IEEE Transactions on Automation Science and Engineering*, vol. 20, no. 2, 2023, pp. 909–922, https://doi.org/10.1109/tase.2022.3171795.

[10] Accepted by the IEEE Conference on Robotics and Automation, London, UK, June, 2023: Automating Vascular Shunt Insertion with the dVRK Surgical Robot. Karthik Dharmarajan, Will Panitch, Muyan Jiang, Kishore Srinivas, Baiyu Shi, Yahav Avigal, Raven Huang, Thomas Low, Danyal Fer, and Ken Goldberg.

[11] Fiorini, Paolo, Ken Y. Goldberg, Yunhui Liu, and Russell H. Taylor. "Concepts and Trends in Autonomy for Robot-Assisted Surgery." Proceedings of the IEEE 110, no. 7 (2022): 993-1011.

[12] Bonne, Sophea, Will Panitch, Karthik Dharmarajan, Kishore Srinivas, Jerri-Lynn Kincade, Thomas Low, Bruce Knoth et al. "A Digital Twin Framework for Telesurgery in the Presence of Varying Network Quality of Service." In 2022 IEEE 18th International Conference on Automation Science and Engineering (CASE), pp. 1325-1332. IEEE, 2022.

[13] Hwang, Minho, Brijen Thananjeyan, Samuel Paradis, Daniel Seita, Jeffrey Ichnowski, Danyal Fer, Thomas Low, and Ken Goldberg. "Efficiently calibrating cable-driven surgical robots with RGBD fiducial sensing and recurrent neural networks." IEEE Robotics and Automation Letters 5, no. 4 (2020): 5937-5944.

[14] Dharmarajan, Karthik, Will Panitch, Muyan Jiang, Kishore Srinivas, Baiyu Shi, Yahav Avigal, Huang Huang, Thomas Low, Danyal Fer, and Ken Goldberg. "Automating Vascular Shunt Insertion with the dVRK Surgical Robot." arXiv preprint arXiv:2211.02293 (2022).

[15] Paradis, Samuel, Minho Hwang, Brijen Thananjeyan, Jeffrey Ichnowski, Daniel Seita, Danyal Fer, Thomas Low, Joseph E. Gonzalez, and Ken Goldberg. "Intermittent visual servoing: Efficiently learning policies robust to instrument changes for high-precision surgical manipulation." In 2021 IEEE International Conference on Robotics and Automation (ICRA), pp. 7166-7173. IEEE, 2021.

[16] Hwang, Minho, Jeffrey Ichnowski, Brijen Thananjeyan, Daniel Seita, Samuel Paradis, Danyal Fer, Thomas Low, and Ken Goldberg. "Automating Surgical Peg Transfer: Calibration With Deep Learning Can Exceed Speed, Accuracy, and Consistency of Humans." IEEE Transactions on Automation Science and Engineering (2022)

[17] Hwang, Minho, Brijen Thananjeyan, Daniel Seita, Jeffrey Ichnowski, Samuel Paradis, Danyal Fer, Thomas Low, and Ken Goldberg. "Superhuman surgical peg transfer using depth-sensing and deep recurrent neural networks." arXiv preprint arXiv:2012.12844 (2020).

[18] Lu, J., Jayakumari, A., Richter, F., Li, Y. and Yip, M.C., 2020. Super deep: A surgical perception framework for robotic tissue manipulation using deep learning for feature extraction. arXiv preprint arXiv:2003.03472.

[19] Huang, J., Liu, F., Richter, F. and Yip, M.C., 2021. Model-Predictive Control of Blood Suction for Surgical Hemostasis using Differentiable Fluid Simulations. arXiv preprint arXiv:2102.01436.

[20] Liu, F., Li, Z., Han, Y., Lu, J., Richter, F. and Yip, M.C., 2020. Real-to-Sim Registration of Deformable Soft Tissue with Position-Based Dynamics for Surgical Robot Autonomy. arXiv preprint arXiv:2011.00800.

[21] Richter, F., Shen, S., Liu, F., Huang, J., Funk, E.K., Orosco, R.K. and Yip, M.C., 2021. Autonomous robotic suction to clear the surgical field for hemostasis using image-based blood flow detection. IEEE Robotics and Automation Letters, 6(2), pp.1383-1390.

[22] Chiu, Zih-Yun, Albert Z. Liao, Florian Richter, Bjorn Johnson, and Michael C. Yip. "Markerless suture needle 6d pose tracking with robust uncertainty estimation for autonomous minimally invasive robotic surgery." In 2022 IEEE/RSJ International Conference on Intelligent Robots and Systems (IROS), pp. 5286-5292. IEEE, 2022.

[23] Rasmussen, Todd, et al. “Vascular Injury (CPG ID: 46).” *Joint Trauma System Clinical Practice Guideline*, vol. 46, 12 Aug. 2016.

Appendix A: Vessel Grasp Location Equations

Figure 38 shows the notation used in the grip-points calculations. This notation is specific to the Operator Control Unit (OCU) aka the remote side. Similar notation is used on the robot side.

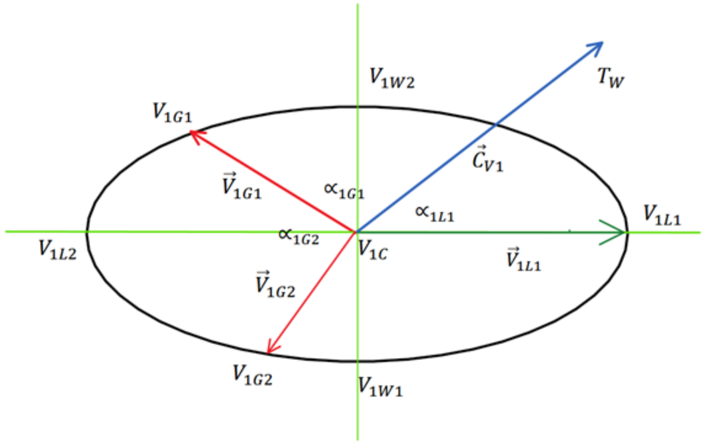

Figure 38. diagram of grip locations along the ellipse of the vessel edge.

The ellipse in Figure 38 presents a lip of the severed vessel. Various points on the ellipse are shown in the diagram and defined below:

T_W is the implicit optical center of the robot's stereo camera pair
V_{1L2}, V_{1L1} are the limits of the ellipse's major axis
V_{1W1}, V_{1W2} are the limits of the ellipse's minor axis

$\vec{C}_{V1}$ is the vector from the centerpoint of the cameras' lenses to the center of the ellipse. $\vec{C}_{V1}$ is projected to the plane of the ellipse.
$\vec{V}_{1G1}$ is the vector from the center of the ellipse to grip point 1 (V_{1G1})
$\vec{V}_{1G2}$ is the vector from the center of the ellipse to grip point 2 (V_{1G2})

α_{1G1} is the angle from projected $\vec{C}_{V1}$ to $\vec{V}_{1G1}$
α_{1G2} is the angle from projected $\vec{C}_{V1}$ to $\vec{V}_{1G2}$
α_{1L1} is the angle from $\vec{V}_{1L1}$ to $\vec{C}_{V1}$ (the angle from the ellipse's major axis to the camera's line of sight)

The virtual OCU displays the simulated vessel using Unreal Engine (UE) as shown in Figure 21. The simulated vessel in the OCU is the only visualization the remote surgeon sees apart from a transparent ghost-like forceps tool representing the location of the lead surgeon's tool identified by the OptiTrack system. The remote surgeon can see when the lead surgeon has grasped the vessel by being represented on the simulated vessel on their OCU and can then initiate their grasp commands by gripping the simulated vessel in their OCU at desired locations. Those locations on the simulated vessel are then translated and the robot is then directed to grasp in the corresponding 3-D locations on the real vessel through the following calculations:

Consequently, the world coordinates of the vessel features as well as the optical camera center (T_W) can be read from UE. Thus, $V_{1L1}, V_{1L2}, V_{1W1}, V_{1W2}, V_{1C}, and\ T_W$ are all available from UE.

The TRON system then needs to calculate the ellipse's plane. Subsequent calculations involve the plane the ellipse lies in (in world coordinates). Given that the values that define in the ellipse are known, the ellipse's plane can be computed. One can use the equation of a plane to calculate the coefficients $(a_e, b_e, c_e, d_{e)})$ for the plane using three points and three equations:

$$a_e * (x_{e_1}) + b_e * (y_{e_1}) + c_e * (z_{e_1}) + d_e = 0$$
$$a_e * (x_{e_2}) + b_e * (y_{e_2}) + c_e * (z_{e_2}) + d_e = 0$$
$$a_e * (x_{e_3}) + b_e * (y_{e_3}) + c_e * (z_{e_3}) + d_e = 0$$

In our case, the three points can be, for example: V_{1C}, V_{1L1}, V_{1W1}. Set d_e to a non-zero value and compute $a_e,\ b_e\ and\ c_e$ using the values of the points that are specified in Unreal Engine. The system then calculates the normal vector to the ellipse's plane. The vector normal to the plane is needed for other calculations. It is computed using the cross product:

$$\vec{n} = \vec{V}_{1L1} * \vec{V}_{1W2}$$

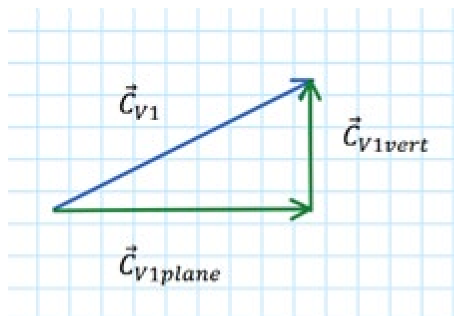

Figure 39. Project $\vec{\boldsymbol{C}}_{\boldsymbol{V1}}$ to the Ellipse's Plane

The vector $\vec{C}_{V1}$ originates in the center of the ellipse on the ellipse's plane and extends to a viewpoint above and distant from the ellipse's center. Project this vector onto the ellipse's plane by projecting the $\vec{C}_{V1}$ vector onto $\vec{n}$ to compute $\vec{C}_{V1vert}$ (the vertical component of $\vec{C}$ that is orthogonal to the plane of the ellipse and pointing out of the page). $\vec{C}_{V1vert} = \vec{C}_{V1} \cdot \vec{n}$ Then subtract $\vec{C}_{V1vert}$ from $\vec{C}$ to get the projection onto the plane $\vec{C}_{V1plane} = \vec{C}_{V1} - \vec{C}_{V1vert}$. The system then adds the base of the projected vector in world coordinates to origin of the projected vector to convert the projected vector to world coordinates. The next steps are to calculate a transformation between the world coordinate system and the coordinate system in the plane that the ellipse lies in and is centered in the center of the ellipse. First, we define the unit vector normal to the x,y plane in world coordinates: $\vec{r} = \{0,0,1\}$. A quaternion, q, can be computed using the unit normal for the two planes. That quaternion transforms coordinates from the ellipse's plane to world coordinates. The quaternion rotates a vector, $\vec{s}$, from coordinates in the ellipse's plane to world coordinates. $\overrightarrow{s'} = q\vec{s}q^{-1}$. In our case, the quaternion is used to convert points on the ellipse between world coordinates and ellipse coordinates.

The last steps involve calculating ellipse perimeter points that correspond to an angle. α_{1g1} is the angle from $\vec{C}_{V1plane}$ to $\vec{V}_{1G1}$. Compute the (x,y,z) coordinates of the point V_{1G1}(the point at the end of $\vec{V}_{1G1}$). The perimeter of the ellipse satisfies the equation : $\frac{x^2}{a^2} + \frac{y^2}{b^2} = 1$. Where a and b are one-half the lengths of the major and minor axes respectively (in the plane of the ellipse, the z value for every point on the perimeter is 0). Referring back to Figure 38, we can calculate V_{1G1} using α_{1L1} and α_{1G1}:

$$V_{1G1} = (V_{1G1x}, V_{1G1y})$$

$$V_{1G1x} = Len(V'_{1L1}) * \cos(\alpha_{1L1} + \alpha_{1G1})$$

$$V_{1G1y} = Len(V'_{1L1}) * \sin(\alpha_{1L1} + \alpha_{1G1}))$$

Where Len(v) is the length of the vector v. Once we have calculated $V_{1G1} = (V_{1G1x}, V_{1G1y})$, which is a point on the ellipse as defined in the ellipse's plane, convert that point to world coordinates by calculating the rotation of that vector using the quaternion calculated in the pervious section.